

Pleistocene-Holocene tectonic reconstruction of the Ballık travertine (Denizli Graben, SW Turkey): (de)formation of large travertine geobodies at intersecting grabens

Koen VAN NOTEN^{1,2,4,*}, Savaş TOPAL³, M. Oruç BAYKARA³, Mehmet ÖZKUL³,
Hannes CLAES^{4,♦}, Cihan ARATMAN^{3,4} & Rudy SWENNEN^{4,*}

¹ *Geological Survey of Belgium, Royal Belgian Institute of Natural Sciences, Jennerstraat 13, 1000 Brussels, Belgium*

² *Seismology-Gravimetry, Royal Observatory of Belgium, Ringlaan 3, 1180 Brussels, Belgium*

³ *Department of Geological Engineering, Pamukkale University, 20070 Kınıklı Campus, Denizli, Turkey*

⁴ *Geodynamics and Geofluids Research Group, Department of Earth and Environmental Sciences, Katholieke Universiteit Leuven, Celestijnenlaan 200E, 3001 Leuven, Belgium*

[♦] *now at Clay and Interface Mineralogy, Energy & Mineral Resources, RWTH Aachen University, Bunsenstrasse 8, 52072 Aachen, Germany*

*Corresponding authors

koen.vannoten@seismology.be (K. Van Noten)

rudy.swennen@kuleuven.be (R. Swennen)

Highlights:

- A new fault map of the entire eastern margin of the Denizli Basin is presented
- Pleistocene travertine deposition occurred along an already present graben morphology
- Dominant WNW-ESE normal faults reflect dominant NNE-SSW extension
- Ballık area acted as a transfer zone during transient NW-SE extension
- Complex fault networks at intersecting basins are ideal for creating fluid conduits

Graphical Abstract: See Figure 14

31 **Abstract**

32 The Ballık travertine geobody developed at the intersection of the NE margin of the Denizli Graben-
33 Horst System (DGHS) and the neighbouring Baklan Graben. To investigate the formation of
34 travertine geobodies and the development and reactivation of faults at intersecting grabens, travertine
35 and faults were mapped in 35 travertine quarries that excavate the NE Denizli margin. The upper
36 margin of the Ballık area comprises a subhorizontal travertine facies that is covered by siliciclastics
37 that likely sourced from the uplifted margin flank north of the Ballık travertine. The travertine in the
38 lower regions start with a similar subhorizontal facies but becomes more complex and evolves to
39 travertine facies formed by a sloping topography with a domal architecture. Travertine precipitated
40 from resurfaced carbonate-precipitating fluids, directly along the margin faults and the fracture
41 network and diffuse through Neogene unconsolidated underlying sediments. From the Denizli basin
42 floor to the uplifted graben shoulders, fault orientation is dominantly WNW-ESE oriented with major
43 basin faults showing a left-stepping trend. Paleostress inversion of fault-slip data reveals that a long-
44 lived, NNE-SSW extensional-transtension phase initiated the WNW-ESE oriented, graben-facing
45 normal fault network in the Early Pleistocene. In the Middle Pleistocene, the Ballık area subsequently
46 acted as a transfer zone between the neighbouring Baklan Basin and NE-SW oriented margin-
47 bounding faults of the DGHS, during which the Ballık fault network was left-lateral strike-slip
48 reactivated. In this period other large travertine geobodies precipitated along Baklan Graben margin
49 faults. Earthquake focal mechanisms, underground spring travertine and fissure ridge orientation
50 indicate a Late Pleistocene-to-current NNE-SSW extensional stress regime during which travertine
51 precipitation moved to more central parts of the DGHS. Large travertine geobodies more likely form
52 at graben intersections because they are susceptible to an enhanced fluid flow sourced from a complex
53 fault-fracture network induced by recurrent stress permutations and fault reactivation during different
54 tectonic regimes.

55

56 **Keywords:** travertine facies development; fault mapping; extension; transtension; strike-slip
57 reactivation; paleostress analysis

58

59

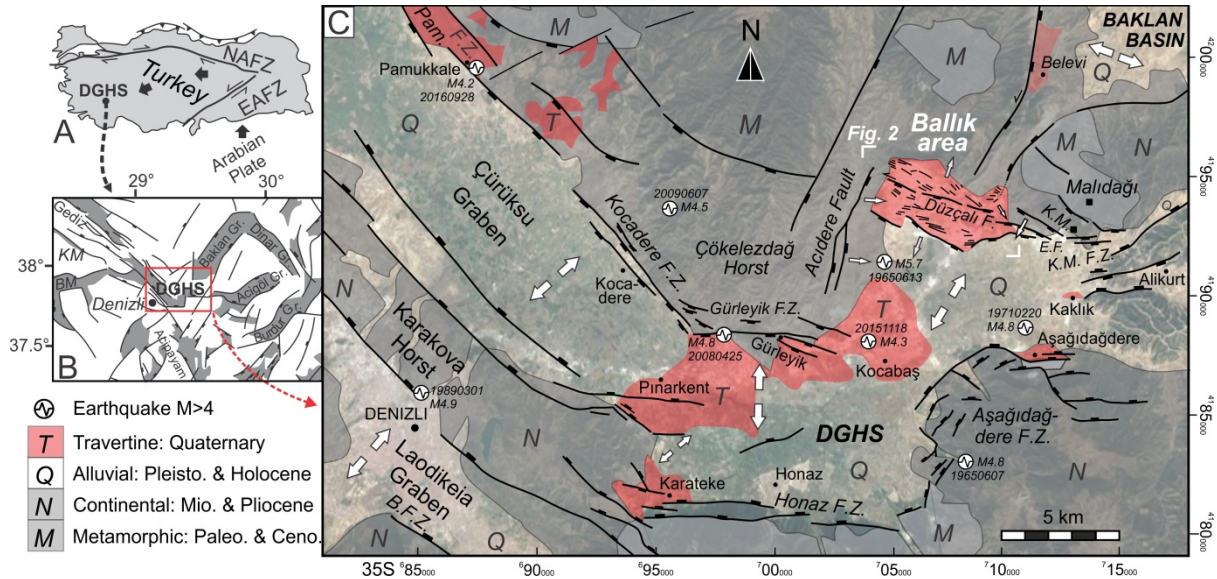
60 **1. Introduction**

61 In situ reservoir characterization is most often based on the combination of seismic and core data. In
62 particular for complex carbonate reservoirs, the sedimentological and tectonic features between core
63 and seismic-scale are decisive for production. Outcrop analogue studies cover this scale-gap and their
64 integration is thus indispensable in multidisciplinary complex carbonate reservoir characterization.
65 Most carbonate reservoirs are naturally fractured from micro- to kilometre scale with fractures acting
66 as highways for fluids in the reservoir. After cementation, however, they can also result in
67 compartmentalisation. A proper understanding of the reservoir-scale fracturing behaviour is thus
68 essential. Among continental carbonate reservoir analogues, travertines best represent the close
69 interaction between sedimentation, crustal fluid circulation and, especially, neotectonic deformation in
70 actively deforming tectonic regions (Hancock et al., 1999). The morphology or reservoir architecture
71 of travertines is controlled by the paleo-topography. In addition, the depositional environment and
72 facies classification in travertines and tufas are also based on paleo-topography, i.e. in the mound
73 versus slope vs depression depositional environment (Guo and Riding, 1998). The paleo-topography
74 itself is, however, strongly dependent on regional and local faulting, affecting spring water discharge
75 and spring orifices that generated the necessary slopes to allow superficial fluid flow. Travertines are
76 thus a prime example of neo-tectonic indicators. Hence, in order to deduce the paleotopography,
77 possible tectonic tilting has to be taken into account. Sedimentological features can be used to deduce
78 tectonic tilting. Conversely, tectonic tilting has to be deduced before interpretation of sedimentology,
79 like paleo-flow direction, is possible. To properly interpret sedimentological analyses and reconstruct
80 complex travertine build-ups, a detailed tectonic analysis thus always needs to accompany travertine
81 sedimentology. Analysing the sedimentology and tectonic deformation of travertine occurrences
82 allows to reveal the nearby presence of the fault-fracture network in the subsurface that provided the
83 necessary fluid pathways, which may have interacted with basement rocks.

84

85 In actively deforming regions, faults control the occurrence, size and geometry of travertine deposits.
86 Geometrically, travertines occur as isolated individual elongate fissure ridges and as (large) travertine
87 geobodies deposited in flat pools or in slope-controlled travertine mounds. Whereas travertine growth
88 along fissure ridges is considered to develop episodically (e.g. Mesci et al., 2008), with fluid
89 expulsion and fissure propagation being impacted by earthquake activity (Brogi and Capezzuoli,
90 2014), large-scale travertine depositions can last for several thousands of years, being fed by an
91 actively enhanced fault-fracture network. Structurally, travertines develop in the fractured
92 hangingwall of normal faults (Altunel, 1994; Brogi, 2004; Brogi and Capezzuoli, 2009; Brogi et al.,
93 2010; De Filippis and Billi, 2012; Brogi and Capezzuoli, 2014; Özkul et al., 2014), in shear zones
94 (Faccenna, 1994; Faccenna et al., 2008), above fault tips or near their lateral end (Çakır, 1999; Kele et
95 al., 2008), but the largest masses can develop in strain-releasing step-overs and along relay ramps

96 developed between margin-bounding faults (Altunel and Hancock, 1993b; Çakır, 1999; Hancock et
 97 al., 1999; Martínez-Díaz and Hernández-Enrile, 2001; Brogi et al., 2012; Temiz et al., 2013). Not only
 98 the travertine outline reveals the geometry of the underlying fault system, also systematic joints and
 99 faults cutting through the travertine can be used as stress indicators for the contemporary tectonic
 100 stress field that has affected the travertine area, either during or after deposition (Altunel, 1994;
 101 Kaymakçı, 2006). Joint propagation and morphology is hereby strongly influenced by the internal
 102 heterogeneity of the travertine (Hancock et al., 1999; Van Noten et al., 2013).
 103



104
 105 **Figure 1:** Geodynamic setting of the study area. **A)** Location of the Denizli Graben-Host System (DGHS) in
 106 Turkey. NAFZ: North Anatolian Fault Zone, EAFZ: East Anatolian Fault Zone. **B)** Overview of sedimentary
 107 basins in the West Anatolian Extensional Province. BM = Büyük Menderes Graben; KM: Küçük Menderes
 108 Graben. **C)** Fault map of the eastern DGHS. Faults are derived from geomorphology and from Koçyiğit (2005).
 109 The Ballık study area is located along the northern graben flank in the eastern part of the DGHS. Minor faults
 110 drawn in the Ballık area are discussed in this study. Different extension directions that have affected the DGHS
 111 are indicated. Location of the M5.7 13 June 1965 earthquake is taken from Westaway (1993), other earthquakes
 112 are taken from the USGS earthquake database. K.M.: Küyükmalı Mountain; E.F.: Elmali fault. B.F.Z.:
 113 Babadağ Fault Zone. Map coordinates are in UTM (35S, WGS 84). Basemap © Google Earth™.
 114

115 Travertine occurrences in the Denizli Graben-Host System (DGHS, Koçyiğit, 2005) in the West
 116 Anatolian Extensional Province (WAEP, southwest Turkey; Fig. 1A, B) are one of the best studied
 117 around the world. In the DGHS, the touristic UNESCO Pamukkale ‘cotton castle’ travertine, actively
 118 precipitating along the Pamukkale Fault Zone, is the most famous example. In the Pamukkale area,
 119 fault, fracture and fissure mapping and their relationship to seismic activity has been studied to link
 120 travertine deposition to the neotectonic context of the Denizli area (Altunel and Hancock, 1993b; a;
 121 1996; Hancock et al., 1999; Özkul et al., 2002; Koçyiğit, 2005; Kaymakçı, 2006; De Filippis et al.,
 122 2012; De Filippis et al., 2013; Özkul et al., 2013; Brogi et al., 2014).
 123

124 Recently, the large-scale Pleistocene Ballık travertine geobody (12.5 km²), which was deposited along
 125 the northeastern step-like faulted northern margin of the DGHS (Fig. 1C), received much attention as

126 reservoir analogue. In this region, travertines are both present along the uplifted margin flank and at
127 the foot of the margin where they are exposed in a large, 2 km-long, ~70 m high, travertine domal
128 structure (further referred to as the *Killik dome*) that developed on top of the ancient Neogene and
129 Pleistocene basin fill. The fact that such a domal structure resembles to aggradational carbonate build-
130 ups in Pre-Salt plays offshore Brazil (Buckley et al., 2013), in the Namibe Basin (Sharp et al., 2013)
131 and offshore Angola (Saller et al., 2016) has increased the interest in the Ballık travertine as a
132 potential reservoir analogue (Claes et al., 2015; De Boever et al., 2016). Along the northern and
133 southern margin of the DGHS, margin-bounding faults are mostly characteristic of pure normal
134 faulting or normal faulting with a small oblique-slip component (Altunel, 1994; Çakır, 1999;
135 Koçyiğit, 2005; Kaymakçı, 2006). Several normal faults, (sub)parallel to the margin-bounding faults,
136 cross-cut the domal structure in the Ballık area. Uncommon with respect to other margin-bounding
137 faults or to focal mechanisms of recent earthquakes (Irmak, 2013), many purely strike-slip kinematic
138 markers are present in the fault infill in the Killik dome (Van Noten et al. 2013). Strike-slip faulting
139 has only rarely been observed in the DGHS. Altunel (1994) reported sinistral strike-slip faults
140 offsetting man-made channels and structures at Hierapolis (Pamukkale) and a few minor WNW-
141 striking strike-slip faults cutting through the fissure ridge at Koçabas. Van Noten et al. (2013)
142 interpreted strike-slip faulting affecting the Killik dome to have occurred during a transient strike-slip
143 stress field in the Pleistocene hereby reactivating the already existing normal faults. However, to date
144 any link with a larger-scale regional tectonic model is still lacking and needs to be addressed.

145 Travertines are not only restricted to the Killik dome but dominate the entire northeastern
146 upper graben flank of the DGHS. Altunel (1994) was the first to study these faults. Although these
147 travertine masses constitute the largest part of the Ballık area and are intensively quarried, they hardly
148 received any attention after Altunel's pioneering study. A detailed fault mapping and tectonic analysis
149 of the entire NE Denizli graben flank was never performed. East and west of the Killik dome,
150 travertine sequences consist mostly of subhorizontal bedded travertine that laterally extends for a few
151 hundreds of meters. Also along the northern flank many lateral intercalations of fluvial conglomerate,
152 sandstone, mudstone, paleosol horizons and erosional surfaces occur (Özkul et al., 2002).

153 With the aim of understanding the tectonic evolution of the entire northern graben flank of the
154 Ballık area, a detailed structural analysis of the Ballık travertine is presented in this study. As
155 travertines are heavily quarried in this area and evidences will be progressively removed in the near
156 future, it is essential to document and report all structural features along this graben flank. This study
157 therefore focuses on the orientation of major travertine structures and domes, on fault orientation and
158 fault-slip kinematic data and on the fracture network. After a geometric analysis on the observed
159 faults, a paleostress analysis is performed on the collected kinematic data. The resulting paleostress
160 directions allow deducing if stress variations occurred during the deformation of the entire NE margin
161 of the DGHS. The dip and orientation of the different travertine masses are only briefly described as a
162 detailed facies analysis is beyond the scope of the study. This study provides an overview of tectonic

163 structures that overprinted the travertine deposits which serve as a tectonic framework for studies that
164 further focus on facies analysis, geochemistry and sedimentology of the Ballık travertine from which
165 the travertine geobody architecture can be reconstructed.

166

167 **2. Tectonic framework**

168 *2.1 Turkey geodynamics*

169 The DGHS is a seismically active basin situated in the West Anatolian Extensional Province (WAEP)
170 in SW Turkey (Fig. 1A). The WAEP developed from a complex interaction of large-scale plate
171 tectonics in the Aegean and Anatolian areas. Due to northwards migration of the Arabian Plate, on the
172 one hand, and the northwards roll-back subduction of the African Plate below the Anatolian Plate in
173 the Aegean region, on the other hand, a westwards squeeze-out motion and an anticlockwise rotation
174 affected the Anatolian plate (Fig. 1A) (McKenzie, 1970; Seyitoğlu and Scott, 1996). This movement
175 was the main driver for the exhumation of the Menderes Massif in the Miocene (Westaway et al.,
176 2005; Alçiçek et al., 2007; ten Veen et al., 2009; van Hinsbergen et al., 2010; Gessner et al., 2013).
177 Subsequent tectonic relaxation resulted in the development of a pronounced extensional stress regime
178 in West Anatolia as shown by the predominantly NE-SW to NW-SE trending grabens, cross-grabens
179 and horst-graben structures developed from the Pliocene to the Quaternary (Westaway, 1993;
180 Seyitoğlu and Scott, 1996; Bozkurt, 2001; ten Veen et al., 2009). Most of these margin-bounding
181 seismogenic faults, including the Denizli margin faults, are still active and were responsible for a
182 number of devastating earthquakes in historic and recent times (Taymaz and Price, 1992; Irmak and
183 Taymaz, 2009; Irmak, 2013). The development and destruction of numerous ancient cities in the
184 Denizli area was affected significantly by destructive earthquakes (estimated > M6) (Altunel, 2000;
185 Piccardi, 2007). Continuous earthquake activity along the margin faults has affected the Pliocene to
186 recent deposits near the margin as well as the poorly-lithified Quaternary sediments in the basin
187 creating typical earthquake-related soft-sediment deformation structures (Topal and Özkul, 2014).

188

189 *2.2 The Denizli Graben-Horst System*

190 The DGHS is surrounded by the E-W trending Gediz, Küçük Menderes and Büyük Menderes Grabens
191 in the east, the NW-SE Acıpayam Graben in the south and NE-SW Baklan, Acigöl and Burdur
192 Grabens developed on the Dinar fault in the northeast (Westaway, 1990; 1993; Price and Scott, 1994;
193 Koçyiğit, 2005; Kaymakçı, 2006) (Fig. 1B). High-angle normal faults, expressed as steep topographic
194 scarps, delimit these basins. Many of these conjugate graben systems are consistent with a NE-SW,
195 NW-SE and N-S multidirectional extension (Bozkurt and Sözbilir, 2006; Gürbüz et al., 2012). The
196 horst-graben morphology of the DGHS formed during alternating seismic periods of subsidence and
197 tectonic uplift (Westaway et al., 2005). A full description of the successive lithologies from the

198 Miocene to recent Quaternary alluvial plain basin and travertine deposits can be found in Alçıçek et
199 al. (2007) and Claes et al. (2015).

200 The NW-SE oriented western and central part of the DGHS can be separated into two
201 Quaternary subgrabens, namely the Çürüksu and Laodikeia Grabens, separated by the uplifted
202 Karakova Horst (Kaymakçı, 2006; Topal and Özkul, 2014). The Çürüksu subbasin forms a c. 50 km
203 long basin that is bordered by the Pamukkale normal fault zone in the northeast (Fig. 1B). Along this
204 fault zone several travertine deposits, among which the active UNESCO Pamukkale travertines, are
205 precipitated in kilometer-wide, left-lateral step-over zones that are developed at the end or between
206 different segments of NW-SE-trending normal margin faults (Altunel and Hancock, 1993b; Çakır,
207 1999; Hancock et al., 1999). Along the northern margin, travertine occurrences are present as
208 complex travertine mounds (Altunel and Hancock, 1993a, b; Kele et al., 2011; Özkul et al., 2013) and
209 as small individual fissure ridges which developed above different branches or step-overs of the NW-
210 oriented margin faults (Altunel and Karabacak, 2005; De Filippis et al., 2012, 2013; Özkul et al.,
211 2013; Yalçiner, 2013; Brogi et al., 2014).

212 The Ballık study area is situated at the southeastern end of the DGHS where the basin
213 morphology changes from NW-SE to locally E-W, forming the lateral extend of the Acigöl Graben in
214 the east. This part of the DGHS has a pronounced staircase geometry. The southern border is
215 delimited by the E-W graben-facing, step-like Honaz fault zone that is separated from the Babadağ
216 fault zone by the NW-oriented transfer zone at Karateke (Fig. 1C). The Honaz fault zone is dominated
217 by normal to oblique-slip faults along which slickenlines all point towards the center of the basin,
218 indicative of differential extension rate (Topal, 2012; Özkaymak, 2015). The Aşağıdağdere fault zone
219 is situated at the most southeastern edge of the DGHS and consists of several short, closely-spaced
220 fault segments that are dominated by oblique-slip normal faults (Koçyiğit, 2005). Along the northern
221 margin, the NW-trending Kocadere fault zone is considered to be the prolongation of the Pamukkale
222 fault zone (Fig. 1C). The short E-W to WNW-ESE normal faults NE of Pınarkent belong to the
223 Gürleyik fault zone and mark the transition from the NW-SE trending to the E-W trending orientation
224 part of the DGHS. It is unknown if these smaller faults continue and maintain their trend towards the
225 WNW-ESE oriented travertine fissure ridge at Kocabaş (Hancock et al., 1999; Özkul et al., 2002;
226 Altunel and Karabacak, 2005; De Filippis et al., 2012).

227 Between Kocabaş and the Ballık area, the DGHS has a NW-SE to ENE-WSW orientation
228 (Fig. 2). In the west, this subbasin is bounded by the N-S Acıdere fault which separates the flat
229 Denizli basin floor in the east from the uplifted Çökelezdağ Horst in the west. The Ballık area is
230 situated along the northern margin and is characterised by several closely-spaced, mainly WNW-ESE
231 faults that are mapped and addressed in detail in this study. NE of the study area, the eastern margin
232 fault of the Baklan Graben intersects with the DGHS.

233

234

235 **2.3 Travertine of the Ballık area**

236 The mountain range front at Ballık, situated 25 km ENE from the city of Denizli, can clearly be
 237 recognised on ASTER satellite images, SRTM DEM and Google Earth™ images (see kml in
 238 supplementary material). The Ballık area forms a steep hill which starts at a basin floor altitude of c.
 239 500 m asl. and reaches a maximum height of 877 m in the west at the Taşkestik Tepe (Fig. 2), i.e.
 240 377 m above the current Denizli basin floor resulting from systematic Quaternary uplift. From top to
 241 bottom along the graben flank, travertine deposits are exposed along stepped, SW-, graben-facing
 242 slopes. 35 quarries that have excavated this large area are addressed in this study. The Ballık
 243 travertine, also referred to as the eroded-sheet travertines (sensu Altunel, 1994) or Kocabaş travertine
 244 geobody (Hancock et al., 1999; Khatib et al., 2014; Lebatard et al., 2014), is by far the largest
 245 travertine site in southwest Turkey (12.5 km²) with travertine thickness up to at least 120 m (Özkul et
 246 al., 2013). The Ballık travertine has been widely used around the world since ancient times as a
 247 construction stone due to its good mechanical resistance and durability properties (Çobanoğlu and
 248 Çelik, 2012; Çelik et al., 2014).

249 Based on the morphology of the northern graben flank, a northern upper margin area can be
 250 separated from the Killik dome. The quarries excavating the Killik dome, i.e. the Faber, Ece, Tetik,
 251 Çakmak, İlik, Alimoğlu and Best abandoned (abandoned is further noted as *Ab.*) quarries (see Fig. 2
 252 and kml in Suppl. Mat. for location of the quarries), were already the subject of several
 253 sedimentological and geochemical (Özkul et al., 2013; Khatib et al., 2014; Claes et al., 2015; El
 254 Desouky et al., 2015; Claes et al., 2017b; De Boever et al., 2017), geomechanical (Çobanoğlu and
 255 Çelik, 2012; Çelik et al., 2014), dating (Lebatard et al., 2014), petrophysical (Soete et al., 2015; De
 256 Boever et al., 2016) and structural (Van Noten et al., 2013) studies.

257 The Killik dome is characterised by horizontally bedded travertine at its base that gradually
 258 changes upwards into complex, slope travertines that are dominated by biohermal reed, cascade and
 259 waterfall travertine facies (Özkul et al., 2013; Claes et al., 2015; De Boever et al., 2017). Travertines
 260 precipitated from resurfaced meteoric waters that infiltrated along the margin that was already
 261 affected by a fault-fracture network. Fluids emerged as heated geothermal waters along the margin
 262 faults after having migrated through and interacted with the Lycian basement rocks (Claes et al.,
 263 2015; El Desouky et al., 2015). In a later stage, secondary fluid circulation was established with
 264 meteoric water interacting at depth and precipitated as calcite veins grown in faults and in the
 265 solution-enlarged fracture network cutting the travertine (Van Noten et al., 2013; El Desouky et al.,
 266 2015).

267

268 **3. Methodology**

269 The northern graben flank was investigated during an extensive field campaign in 2014 and several
 270 revisits in 2015 and 2016. Our study focuses on brittle structures such as joints (barren fractures

271 without any slip), open fissures (no displacement and infill), faults and fault kinematic indicators
272 including slickensides, slickenlines and displaced travertine lamination and paleosols. The orientation
273 of planar structures is reported as dip direction/dip (*e.g.* P270/80 for a fault plane dipping steeply to
274 the west) whereas linear features are reported as trend/plunge (*e.g.* L090/85 for a slickenline plunging
275 steeply to the east). Fault/fracture orientation analysis is performed with the program Stereo 32
276 (Röller and Trepman, 2003). Kinematic data of faults and fractures collected in the quarries are
277 visualised in lower hemisphere, equal-area projection stereoplots in the figures and raw fault/fracture
278 measurements are available per quarry in Suppl. Mat. S2.

279 Quarries in the Ballık area were systematically investigated for the presence of faults. The
280 2013 Google EarthTM satellite image was used as basemap in all figures as this compares most closely
281 with actual quarry situation during the main 2014 fieldwork. Due to continuously moving excavation
282 fronts of the active quarries, quarry walls on current Google Earth images may no longer be in the
283 same position as indicated in the figures in this study. Accurately-taken GPS points of individual
284 observations (with a Trimble Geoexplorer GPS) were used to analyse if the position of the analysed
285 excavation fronts was different than that on the Google Earth satellite image. GPS points are indicated
286 on the fault map figures as small white dots to illustrate where faults were observed. Between
287 travertine quarries, these individual fault observations were strategically linked to map out along-
288 strike fault continuity.

289 With the geometrical fault dataset, a paleostress analysis is performed on the collected data.
290 Principal stress directions can be derived from inversion of fault slip kinematic data. Most paleostress
291 inversion techniques assume the Wallace-Bott hypothesis (Wallace, 1951; Bott, 1959), which state
292 that fault slip should occur parallel to the resolved shear stress on a pre-existing or newly formed fault
293 plane. Inversion of fault-slip data involves the concept of deriving a best-fitting tensor that can
294 explain the direction of slip of the observed faults. The paleostress tensor and the principal stress
295 directions responsible for the (re)activation of the observed faults were derived from the Right
296 Dihedral Method (Angelier and Mechler, 1977) optimised in the Win-Tensor Program (version 5.0.2).
297 This program has the advantage that based on their kinematic features, different phases of faulting can
298 be separated semi-automatically. The different applied steps and quality control of paleostress
299 inversion are described in Delvaux and Sperner (2003) and in Kipata et al. (2013).

300

301 **4. Tectonic analysis of the Ballık area**

302 To facilitate the description of the structural features, we separate the study area in five different
303 domains. This separation is made according to the observed fault kinematics characterising each
304 domain (Fig. 2). The focus is on 1) large-scale faults cutting through the Ballık travertine; 2) the NE
305 extensional domain; 3) the NW extensional domain; 4) the eastern and 5) western extensional and
306 strike-slip reactivated domain; 6) the strike-reactivated domain in the footwall of Düzçalı fault; and 7)

307 the Killik domal area and Southern Ballık area. The fault-fracture deformation for each quarry is
 308 shortly described in this section. All domains, fault data, quarry locations, fault observations and dip
 309 of the studied travertine masses are also presented in a Google Earth™ kmz file provided in
 310 Supplementary Material (S1). Raw fault-fracture orientations are provided for reproducibility in S2.

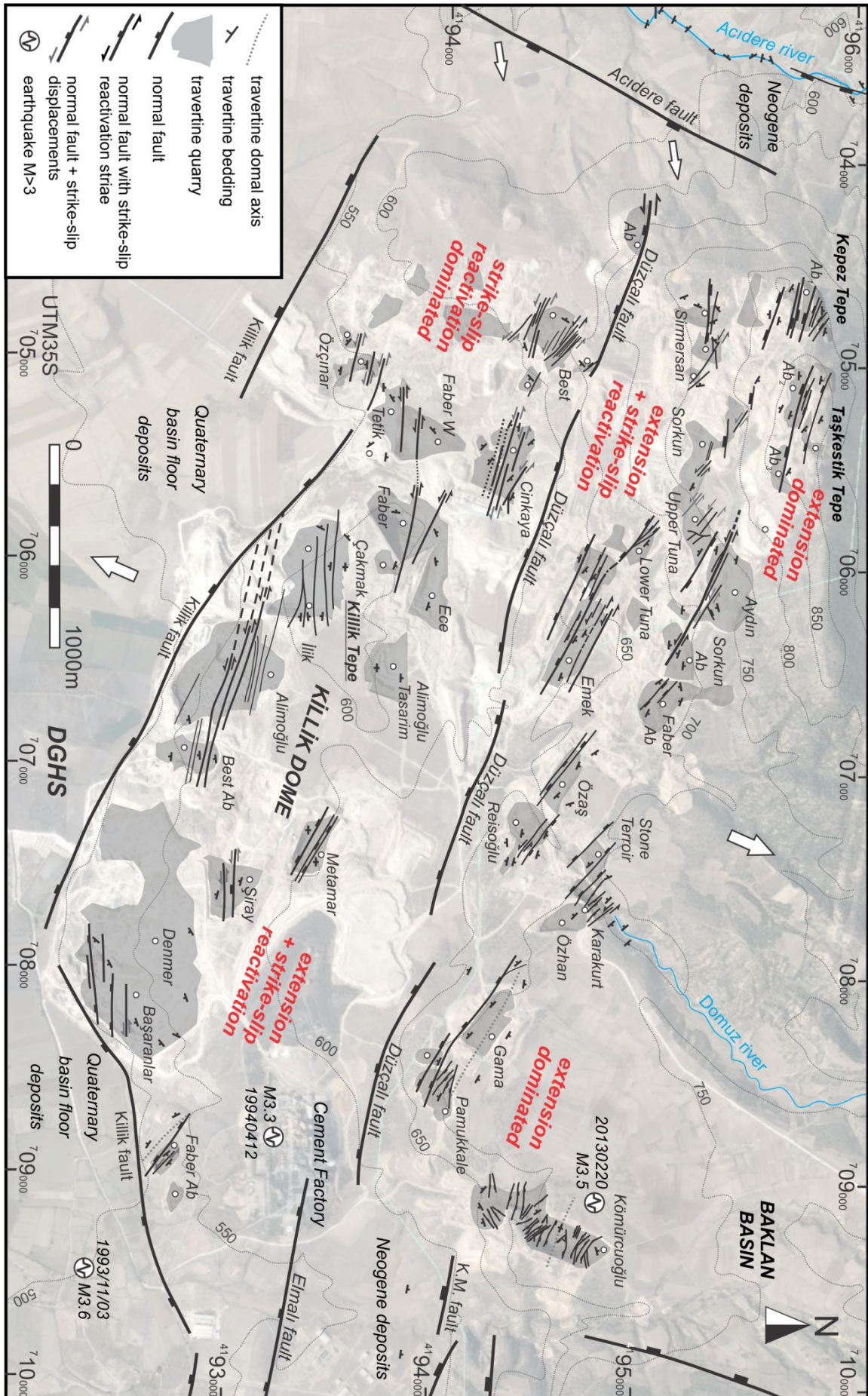
311

312 **4.1 Large-scale faults: The Elmalı, Düzçalı, Killik and Acidere faults**

313 Several kilometre-scale faults cross-cut the Ballık area and can be deduced from the morphology of
 314 the mountain range-front. In the east of the area, the WNW-trending Küçükmalıdağ fault zone
 315 delimits the northeastern incipient margin of the DGHS. This two- to three kilometre wide and 10 km
 316 long fault zone developed at the base of the Küçükmalı and Malıdağ mountains and consists of three
 317 fault sets: i.e. the Düzçalı, the Küçükmalıdağ and Elmalı faults along which Jurassic-Cretaceous
 318 dolomitic limestone, Upper Oligocene conglomerate, Middle Miocene clastics and Quaternary
 319 travertine and alluvial-plain sediments are tectonically juxtaposed (Koçyiğit, 2005). The
 320 **Küçükmalıdağ** and **Elmalı faults** are present east of the travertine excavation area. At the base of the
 321 Küçükmalı mountain (east of the cement factory, see eastern part of Fig. 2), eroded Neogene terraces
 322 dip towards the mountain flank due to activity along the listric Elmalı fault. Although Koçyiğit (2005)
 323 reported that the lateral end of the Elmalı fault should also be present just north of the Denizli Cement
 324 Factory (Fig. 2), no significant geomorphological or tectonic fault traces that support this observation
 325 were found.

326 The **Düzçalı fault** consists of four SW-, graben-facing, left-stepping fault segments of ~1 km
 327 in length. These segments can be traced in the field as the footwall is always a steep hill that consists
 328 of travertine, whereas the hangingwall has a gentle topographic slope along which fan-apron cover
 329 sediments are deposited. According to Koçyiğit (2005) and Altunel (1994), normal displacements
 330 along the Düzçalı fault reach up to c. 200 m. Fault surfaces dominantly contain steeply-dipping
 331 slickensides with only a minor dextral strike-slip component. However, in a small abandoned quarry
 332 at the western end of the Düzçalı fault subhorizontal strike-slip slickenlines (L280/16) overprint older
 333 steeply-plunging dip-slip slickenlines (L285/74) on a fault scarp (Fig. 3A) and indicate fault
 334 reactivation. This observation explains why both normal and strike-slip slickenlines were reported in
 335 the Düzçalı fault orientation analysis of Koçyiğit (2005).

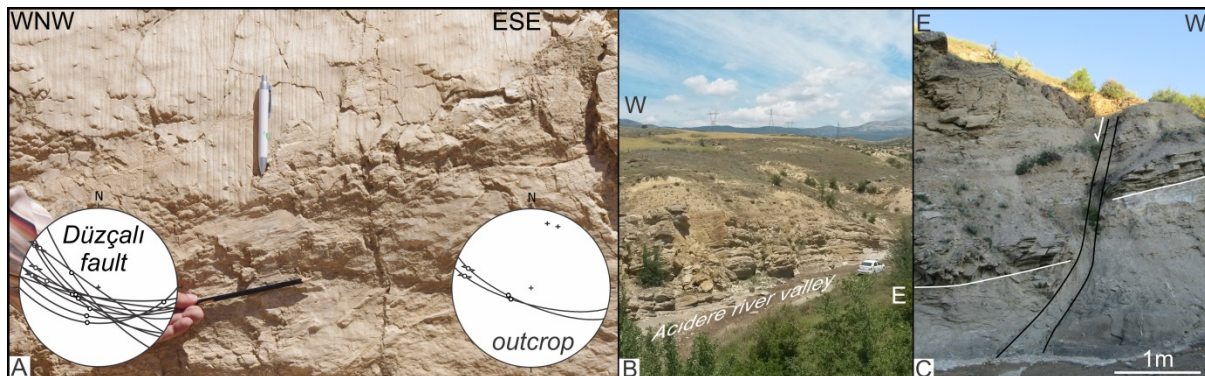
336 Travertine is nowhere further excavated than at the southern border of the Killik dome where
 337 it is bordered by the Killik fault. The **Killik fault** has a dominant WNW-ESE orientation (Fig. 2). In
 338 the east, its orientation changes from WNW-trending to NE- and ENE-trending as a left-lateral step-
 339 over towards the Elmalı fault. In the west, south of the Tetik and Özçınar quarries (Fig. 2), fault
 340 orientation remains NW-SE but its position is translated by 500 m southwards as can be seen by the
 341 change in morphology of the mountain range-front. The Killik and Elmalı faults are considered to be
 342 active as indicated by range-front hydrothermal springs and few small-magnitude earthquakes, such as
 343 for instance the 3 November 1993 M_L 3.6 and 12 April 1994 M_L 3.3 earthquakes.



345 **Figure 2:** Ballık fault map. Grey areas outline the different quarries and refer to the excavation fronts in 2013
 346 (basemap © Google Earth). Coordinates are in UTM 35S. Eye altitude of satellite image is 5.07 km. The
 347 Düzçalı fault segments and the large normal faults bordering the travertine excavation area are derived from
 348 geomorphology and after Koçyiğit (2005). Topographic isohypses are taken from the 1:25 000 Denizli M22-B1-
 349 B4 topographic maps (1989) illustrating the original topography before excavation of the northern flank. White
 350 dots = quarries; Ab = Abandoned quarry; K.M. (F.Z.) = Küçükmalıdağ (Fault Zone); black strike-slip arrows
 351 = observed sinistral displacement; grey strike-slip arrows = inferred sinistral displacement.

353 West of the Ballık area, the DGHS is bordered by the N-S oriented, steeply E-dipping Acıdere normal
 354 fault (Figs. 1 and 2). The Acıdere fault is geomorphologically visible because Quaternary sediments
 355 in the hangingwall form the flat basin floor of the DGHS, whereas the hills and older Neogene
 356 deposits in the footwall are strongly eroded due to the uplift of the Çökelezdağ Horst (Figs. 1 and 2).
 357 The footwall of the Acıdere fault is eroded by the Acıdere river (Fig. 3B). In the Acıdere valley
 358 alternating Oligocene sandstone and mudstone beds are exposed of which bedding alternates between
 359 NW- and W-dipping and is gently folded (see bedding in NW corner of Fig. 2). The fact that these
 360 Oligocene beds tilt to the west is related to backtilting of the Çökelezdağ Horst. Few N-S-trending, E-
 361 facing normal faults (Fig. 3C), i.e. parallel to the Acıdere fault, affect these sediments and
 362 demonstrate the N-S faulted nature of this horst structure.

363



364 **Figure 3:** A) Fault scarp observed at the western tip of the Düzçalı fault in an abandoned quarry in the W
 365 Ballık area. Subhorizontal strike-slip slickenlines (L280/16) overprint steeply-plunging (L285/74) slickenlines.
 366 The right stereoplot displays fault and slickenline orientation in this outcrop. The left stereoplot illustrates all
 367 observations (including also data from Koçyiğit, 2005) of the Düzçalı fault in the Ballık area. B) W-dipping
 368 tilted Oligocene deposits in the Acıdere valley in the footwall of the Acıdere fault, Çökelezdağ Horst. C) N-S
 369 trending, E-facing normal fault affecting Oligocene sandstone and mudstone in the Acıdere valley.

370

371 372 **4.2 NE extensional domain: Kömürcüoğlu, Pamukkale & Gama quarries**

373 In the northeasternmost part of the Ballık area, the **Kömürcüoğlu** travertine is excavated (Figs. 2 and
 374 4). Based on bedding orientation of travertine and the abundant presence of thin paleosols and
 375 intercalating conglomeratic layers, a WNW-ESE-oriented mound travertine structure is recognised.
 376 In the northern part of the quarry, travertine dips gently ($< 10^\circ$) to the NNE. In the central part, the
 377 travertine is sub-horizontal while in the southern part of the quarry, a travertine lobe with a cascade-
 378 and waterfall facies (sensu Claes et al. 2015) dips gently to steeply ($> 30^\circ$) to the SSW (Fig. 4B-B').
 379 The top of the mound structure is covered by clastic sediments including conglomerates (Fig. 5F),

380 sandstone and marls. These sediments thicken from the NW to the SE suggesting a WNW-oriented
381 dip of the top of the mound travertine structure (Fig. 4A-A'). In the southern part of the quarry, a 10
382 m-thick clastic layer of alternating layers of marls and sandstone laterally interfingers with the SSW-
383 dipping end of the travertine structure (Fig. 5A). These layers are covered by subhorizontal travertine.

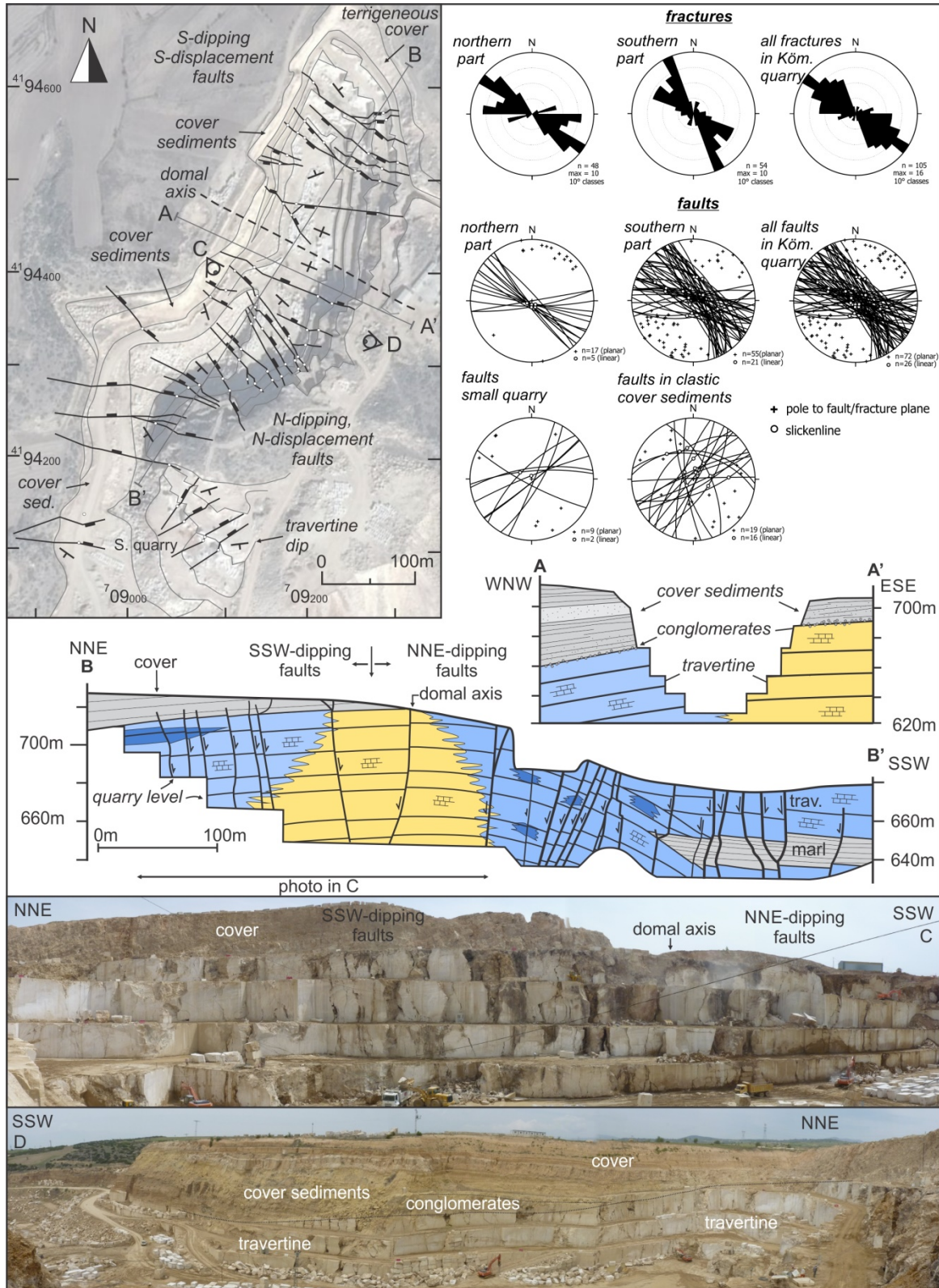
384 The majority of normal faults crossing the K m rc ođlu travertine have a NW-SE
385 orientation. A minor amount is E-W oriented. In the southern part of the quarry faults are vertical to
386 mostly steeply (up to 50°) north-dipping and have a northward normal displacement (Fig. 5B, 5C). In
387 the northern part, all faults are subvertical to steeply south-dipping and have a decimetre- to metre-
388 scale southward normal displacement (Fig. 5F). The location where faults change from N- to S-
389 dipping lies close to the center of the travertine mound structure. Slickenlines on the fault walls are
390 always dip-slip, only slightly deviating from verticality (Fig. 5D). Along strike, faults bifurcate into
391 different fault branches and can have an S-shaped morphology.

392 At the contact between travertine and marl-dominated units, fault orientation refracts due to
393 the ductile behaviour of the marly unit (Fig. 5A). This is the case with the normal faults that cross the
394 interfingering marls (Fig. 4B-B'). Faults/fractures crossing the competent conglomeratic cover layers
395 are very irregular along strike. Due to this irregularity, faults in cover sediments along the eastern
396 quarry flank cannot be connected to the western part. As faults' orientation is irregular, they do not
397 represent the regional extension. Hence, faults in cover sediments are illustrated separately in the
398 orientation analysis in Figure 4 and will not be used for paleostress inversion.

399 Each fault has its own complex formation history. Opposite fault walls are often symmetrical
400 (Fig. 5C) and are typically characterized by multiple succeeding phases of faulting, fault-parallel fluid
401 flow, dissolution, brecciation and developments of striations by mechanical friction (Fig. 5D, E). Each
402 of these different phases can later be cemented due to secondary fluid circulation. The faults are filled
403 by brown oxidised mud, travertine clasts, debris and organic-rich material. The muddy and chaotic
404 infill is indicative of the open nature of the faults during extension, enlarged by dissolution of the fault
405 walls. Slickenlines are not always visible on the fault plane as secondary fluid flow has often
406 overgrown these kinematic markers.

407 In a small quarry south of K m rc ođlu (S. quarry in Fig. 4), the edge of the travertine dome
408 is excavated. Compared to the NW-SE-trending faults in the K m rc ođlu quarry, here, faults have a
409 different NE-SW orientation. The displacement of these faults is, however, still northwards. In this
410 quarry, metre-scale caves emplaced in biohermal reef facies are present (Fig. 5G). These caves are
411 often covered by millimetre- to centimetre-thick alternating brown, white and beige banded secondary
412 wall cements that can be seen around the entire cave. At the top of the cave hanging, pillar-shaped
413 phyto plants are coated by cements giving rise to stalactite-like appearances hanging from the cave
414 ceiling.

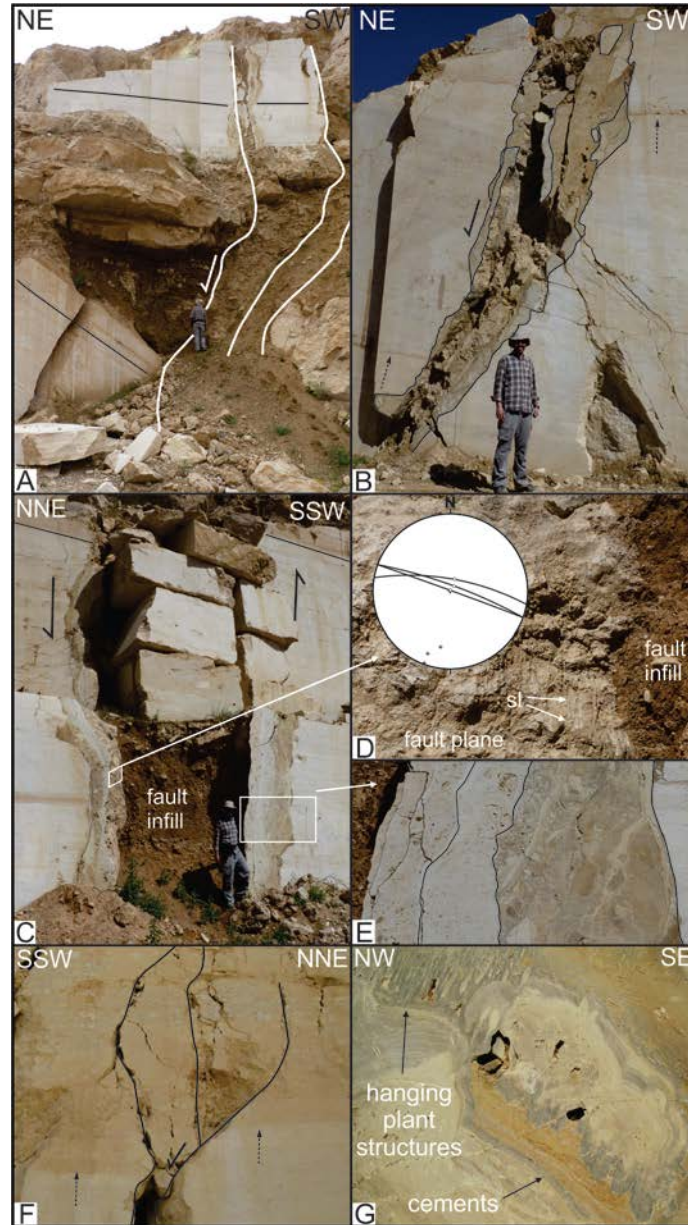
415



416

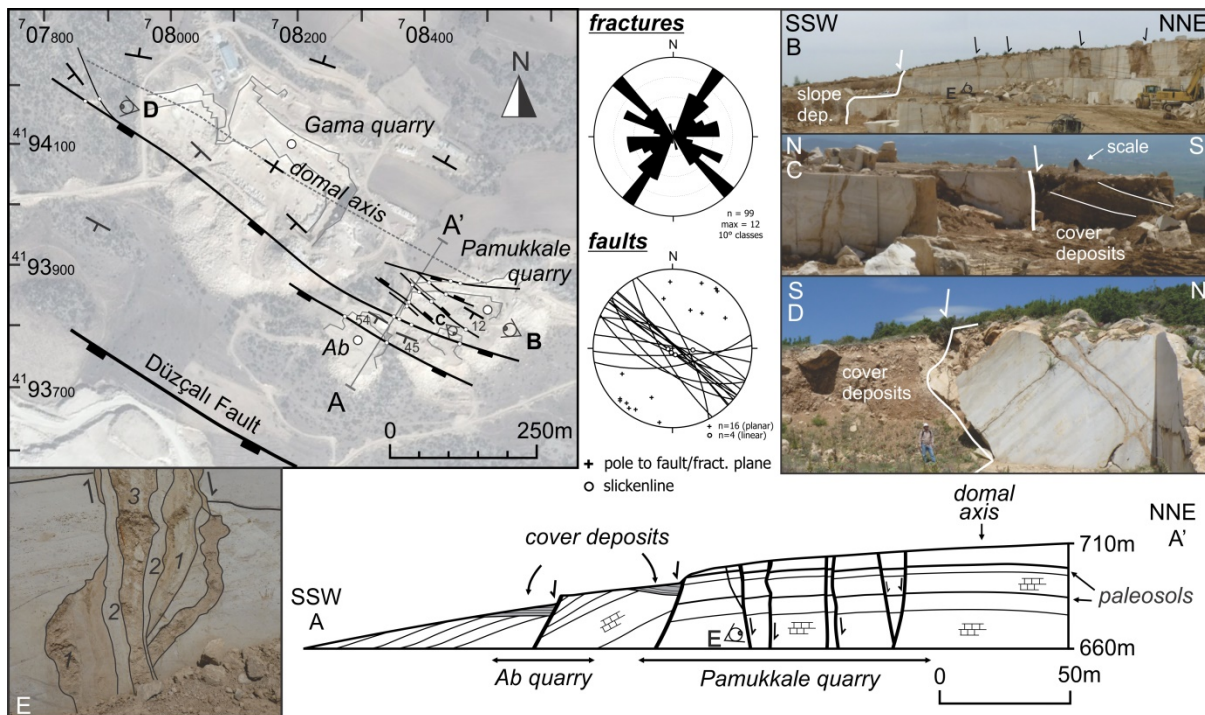
417 **Figure 4:** Fault map (basemap © Google Earth) and fault/fracture kinematic analysis (stereoplots) of the
 418 Kömürcuoğlu quarry (NE Ballık area). Note the different orientation of the faults in the small quarry in the
 419 south (S. quarry). The combined sedimentological and structural model shows that central sub-horizontal
 420 travertines (yellow) laterally continue into sloping cascade (blue) and waterfall facies (dark blue). The northern
 421 part is cut by upright to steeply S-dipping fractures and normal faults, with a southwards displacement, whereas
 422 the southern part is cut by north-dipping faults with northwards displacement. NW-dipping marly, conglomerate
 423 and sandstone (A-A') cover the travertine dome. Marly deposits interfinger with the travertine structure
 424 (southern part of B-B').

425 Joints have similar orientations than the faults. In the northern part of the quarry, joints are vertical
 426 and are NW-SE- to E-W oriented whereas in the southern part, the joints are steeply north-dipping
 427 and have a NW-SE to WNW-ESE orientation. Also a minor population of NE-SW- to NNE-SSW
 428 joints has been observed.
 429



430
 431 **Figure 5:** Kinematic features observed along of the Kömürçuoğlu faults. **A)** Interfingering marls and sandstone
 432 layers in the southern part of the quarry. Note the change in fault orientation when it hits the contact between
 433 clastic sediments and travertine. **B)** Northwards displacement of a normal fault in the S part of the quarry. **C &**
 434 **E)** Open normal fault in the S part of the quarry. Fault walls are characterized by a complex build-up indicative
 435 of multiple phases of faulting, lateral fluid flow and brecciation. The fault is filled by mud and travertine blocks.
 436 **D)** Dip-slip slickenlines (sl) observed in the hangingwall of the fault in c). **F)** Contact between travertine and
 437 conglomeratic cover. Southwards displacement of an N-dipping normal fault in the northern part of the quarry.
 438 **G)** Stalactite-like features hanging from a cave's ceiling. Cavity infill by cement precipitation of hanging plants
 439 observed in the small quarry (S. quarry). Cement infill around the cave.
 440

441 The **Pamukkale** and **Gama** quarries are excavating the hill north of the cement factory (Fig. 3).
 442 Based on bedding and on morphology of the mountain flank, a WNW-ESE trending domal structure
 443 can be recognised with a NNE- and SSW-dipping flank (Fig. 6A-A'). Faults are absent in the Gama
 444 quarry. In the Pamukkale quarry, several small, decimetre-scale displacement normal faults cut the
 445 abundant thin paleosols that are present in the laminated travertine. Faults are vertical to steeply N-
 446 and S-dipping and have a NW-SE trending orientation. This orientation slightly deviates from two
 447 large SW-oriented normal faults that limit the southern edge of the Pamukkale travertine. The
 448 travertine in the hangingwall of these faults is tilted with bedding steeply SW-dipping ($\sim 45^\circ$) (Fig.
 449 6A-A', D).

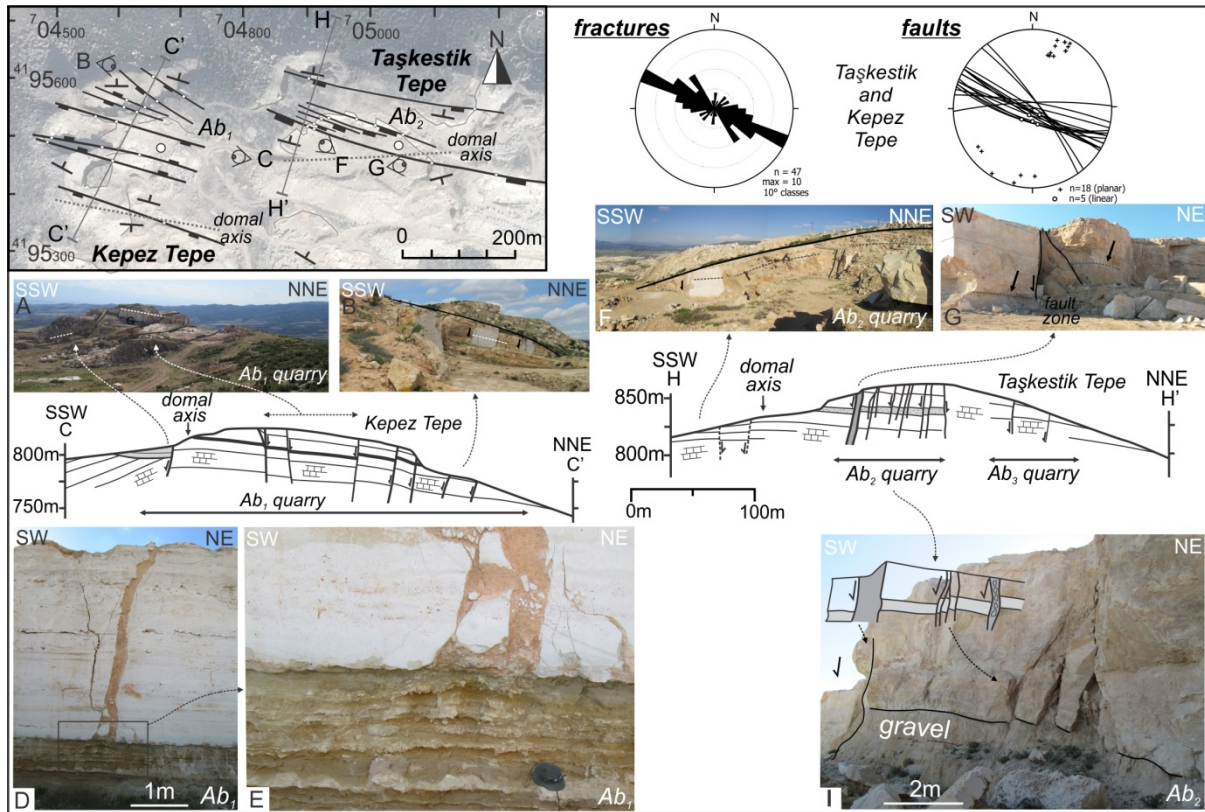


450
 451 **Figure 6:** Fault map (basemap © Google Earth) and kinematic analysis (stereoplots) of normal faults observed
 452 in the Pamukkale and Gama quarries (NE Ballık area). **A-A')** The travertine is cut by normal faults. **B)**
 453 Overview of the Pamukkale quarry and minor normal faults. **C-D)** Two normal faults cut the edge of the
 454 Pamukkale-Gama travertine dome. Note the abrupt change of travertine into slope deposits or marls. **E)**
 455 Complex fault with several deformation and infill phases.

456 Gravity-driven, fan-apron slope deposits, including unsorted, irregularly-oriented travertine blocks set
 457 in a sandy to marly matrix, cover the hangingwalls of these normal faults (Fig. 6B-D). The
 458 slickenlines observed on fault slip planes in these cover deposits are random in orientation indicating
 459 the ductile nature of the marls. These two faults can be followed through the quarry in a NNW-SSE
 460 direction. Fault history is characterised by numerous different stages of fracturing, fluid flow,
 461 brecciation and mechanical friction creating slickenlines (Fig. 6E). Joint population can be subdivided
 462 in three distinct, mutual abutting joint sets which are oriented WNW-ESE (parallel to the observed
 463 faults), NNE-SSW and E-W.

464
 465
 466

467 **4.3 NW extensional domain: Kepez and Taşkestik Tepe**



468 **Figure 7:** Fault map (basemap © Google Earth) and fault/fracture kinematic analysis (stereoplots) of the
 469 Abandoned quarries on the Kepez Tepe and Taşkestik Tepe. **C-C'**) Normal faulting through the travertine on the
 470 Kepez Tepe. Note the change in bedding orientation due to activity along the SSW-most normal fault (**A**) and the
 471 NNE-dipping bedding in Ab_1 (**B**). **D-E**) Dissolution-enlarged and clay-filled fracture cutting the travertine but
 472 arresting on the gravel-travertine contact. **H-H'**) Graben-facing normal faulting affecting the travertine on the
 473 Taşkestik Tepe. Note the 10 m displacement of a thick intercalating gravel layer at the SE end of the picture **I**.
 474
 475

476 At the highest point of the northern graben edge, the **Kepez Tepe** and **Taşkestik Tepe**, two individual
 477 travertine domal bodies, are exposed (Fig. 7). In the NW, a WNW-ESE oriented travertine body was
 478 excavated in an abandoned quarry (Ab_1). Travertine dips gently to the NNE and is cut by WNW-ESE
 479 oriented normal faults (Fig. 7C-C'). Displacement is mostly to the SSW, however, in the middle of
 480 the quarry two faults have a NNE displacement. At the southern end of the travertine mass in Ab_1 ,
 481 bedding is dipping moderately to SSW due to block rotation along a listric normal fault (Fig. 7C-C').

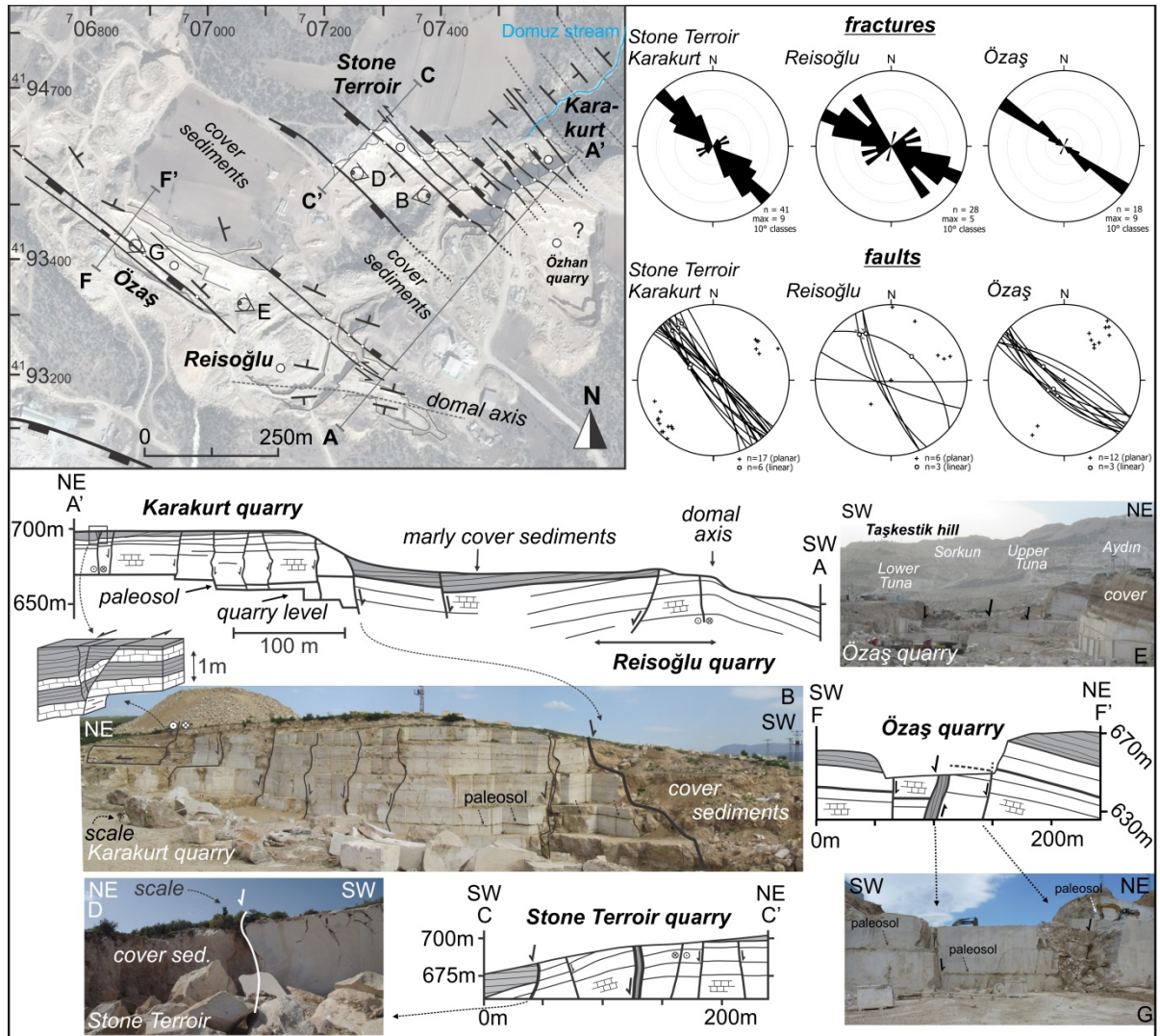
482 A metre-thick gravel layer is present in the travertine. Joints are only limited to the travertine
 483 and arrest at the travertine-gravel boundary. The thick muddy infill of these joints (Fig. 7D, E)
 484 suggests that joints are dissolution enlarged by weathering of the fracture walls.

485 The travertine dome on the **Taşkestik Tepe** is also WNW-ESE oriented and was excavated in
 486 old abandoned quarry (Ab_2). Travertine dominantly dips to the NNE due to block rotation. At its
 487 lateral end, gently SSW-dipping layers are exposed (Fig. 7F, H-H'). SSW-facing normal faults affect
 488 the dome and can have displacements up to 10 m. Normal faults are consistent in orientation and can
 489 be traced for several hundred metres through the different quarries on the Taşkestik Tepe. Joint
 490 orientation is dominantly parallel to the faults.

491
492
493
494
495
496
497
498

4.4 Eastern extensional and strike-slip reactivated domain: Karakurt, Stone Terroir, Reisoğlu, and Özaş quarries

In the Karakurt, Özhan and Stone Terroir quarries a continuous NW-SE oriented, subhorizontal travertine mass is excavated. NE of Karakurt, this travertine mass continues in the small valley of the Domuz river in which bedding alternates between gently NE- and SW-dipping (NE corner in map on Fig. 8). In the four quarries that are described next, the NW-SE oriented fault and joint set is the dominant one.



499

Figure 8: Fault map (basemap © Google Earth) and fault/fracture kinematic analysis (stereoplots) of Karakurt, Stone Terroir, Reisoğlu and Özaş quarries. **A-A'** Cross-section through Karakurt (**B**) and Reisoğlu quarries. In the NE part of Karakurt, a sinistral (transtensional) strike-slip fault with horizontal striae is present. **C-C'** Structure of Stone Terroir quarry. Large normal fault at the SW edge. **D**) Slope deposits cover the hangingwall. **E**) A marly-sandstone sequence covers the Karakurt-Stone Terroir and the Özaş-Reisoğlu travertine bodies. **F-F'** A wide SW-dipping normal fault zone with more than 20 m displacement cuts the NNE-dipping Özaş travertine mass. A 0.5 m-thick paleosol (**G**) and the marly-sandstone cover are displaced over 20 m by this fault.

500
501
502
503
504
505
506
507
508
509

Subvertical NW-SE to NNW-SSE normal faults with decimetre- to metre-scale, alternating NE and SW displacement cut the travertine body in **Karakurt**. The NE part of Karakurt is cut by a

510 south-dipping strike-slip fault. Based on the slickenlines, slickensides and the observed displacement,
 511 a left-lateral fault movement can be deduced. The SW edge of Karakurt is cut by a SW-dipping
 512 normal fault (Fig. 8B) that can be connected to a 5m-wide, open fault zone in the centre of Stone
 513 Terroir (Fig. 8C-C').

514 In **Stone Terroir**, bedding changes from subhorizontal (lateral equivalent of Karakurt) to
 515 gently SW-dipping (~15°), forming the SW edge of the Karakurt-Özhan-Stone Terroir travertine
 516 mass. Fault infill is marked by subhorizontal slickenlines indicative of small-displacement strike-slip
 517 faults. The SW edge of the travertine body is cut by a SW-dipping normal fault (Fig. 8C-C', D). The
 518 travertine in the hangingwall of this normal fault is covered by deposits consisting of muds, marls and
 519 rotated travertine blocks (Fig. 8D). Marly deposits cover the travertine domes of Stone Terroir and
 520 Özaş. Between both quarries these cover deposits are expressed in the landscape as a flat field (Fig.
 521 8F-F').

522 In the upper levels of **Reisoğlu**, a domal axis is visible with bedding oppositely NNE- and
 523 SSW-dipping (Fig. 8A-A'). This travertine body can laterally be followed towards **Özaş** where only
 524 the NE-dipping flank is excavated. A long SW-dipping normal fault is present in the centre of Özaş.
 525 This large normal fault has a c. 20 m SSE-oriented displacement deduced from a 0.5 m-thick paleosol
 526 (Fig. 8E, F-F'). Opposite to this normal fault, a smaller subvertical fault with a NE displacement is
 527 present (Fig. 8G) showing that the travertine in the centre of the Özaş quarry was collapsed due to
 528 extension.

529

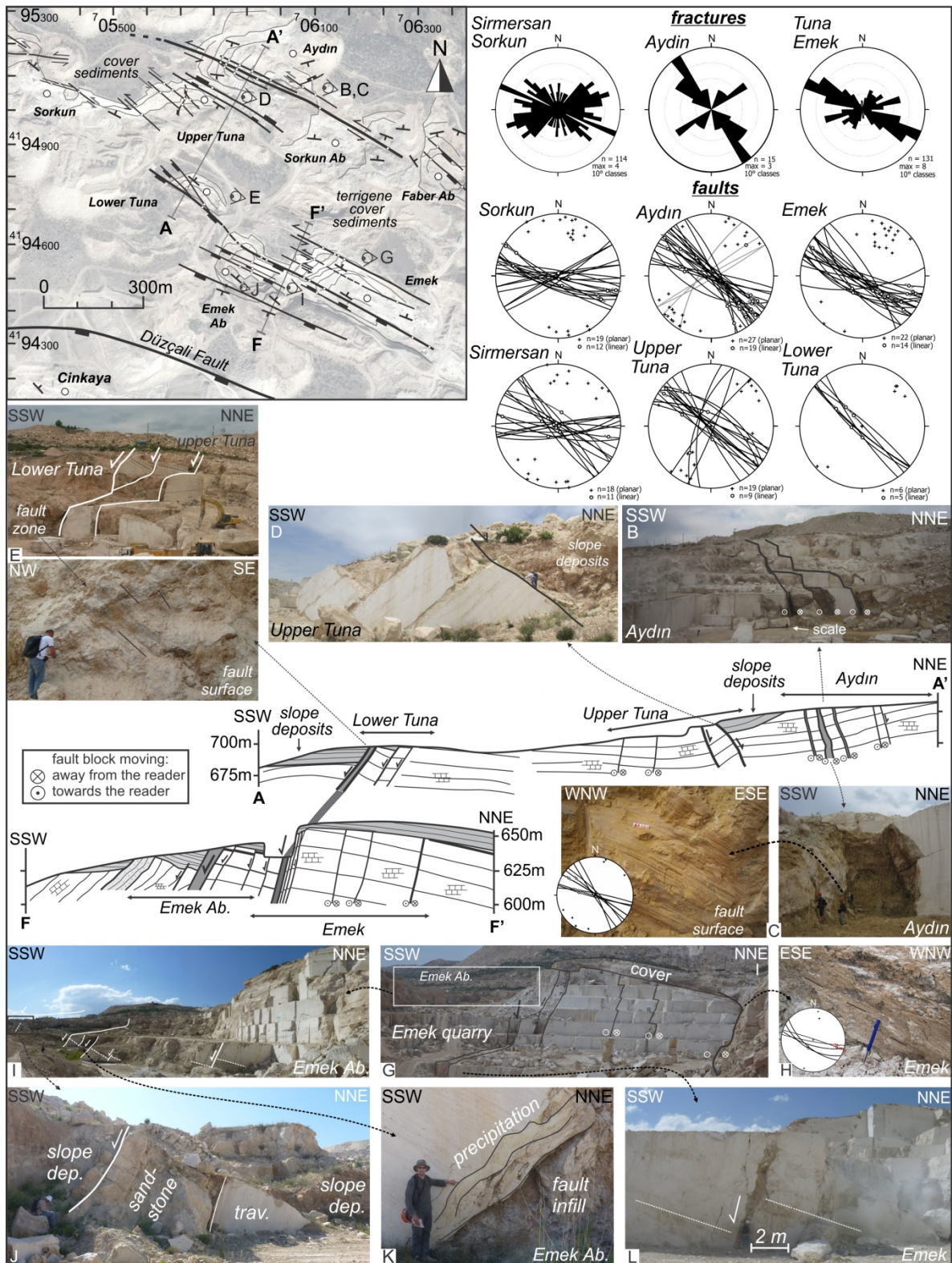
530 **4.5 Western extensional and strike-slip reactivated domain: Aydın, Sorkun, Simersan, Tuna and**
 531 **Emek quarries**

532 At the foot of the Taşkestik Tepe, the Sirmersan, Sorkun, Upper Tuna, Aydın, Sorkun Ab., Faber Ab.
 533 quarries excavate(d) a continuous NW-SE oriented 1.5-km long travertine geobody. Upper Tuna
 534 encompasses three travertine facies, which change from bottom to top from a subhorizontal facies
 535 interfingered with detrital channel facies to a waterfall facies. In Aydın and Upper Tuna travertine
 536 dips gently to the SSW (Fig. 9A-A'). In Upper Tuna, bedding is dominantly subhorizontal, whereas in
 537 the southern part of Upper Tuna and in Sorkun travertine dips gently to the NE. The top of the Sorkun
 538 and Upper Tuna travertine is covered by clastic sediments that can be interpreted as a siliciclastic
 539 channel facies consisting of fluvial conglomerates and marl sediments that wedge with the
 540 subhorizontal travertine facies. The terrace morphology of the Taşkestik Tepe is controlled by these
 541 channel sediments with flat horizontal fields indicative of siliclastic sediments, and steep hills
 542 indicative of travertine.

543 **Aydın** is characterised by three, meters-wide, WNW-ESE-oriented fault zones (Fig. 9B, C)
 544 filled with mud and travertine blocks. Slickenline orientation ranges from subhorizontal with a NW-
 545 SE trend, to gently SE- and NW-plunging, indicative of strike-slip and oblique-slip faulting.

546

547



548

549 **Figure 9:** Fault map (basemap © Google Earth) and kinematic analysis (stereoplots) of faults in the Emek,
 550 Lower and Upper Tuna, Aydın, Sorkun and Sirmersan quarries (NW Ballık area). **B & C)** Metre-wide, open
 551 strike slip fault zones with gently plunging slickenlines in Aydın. **D)** Block rotation in Upper Tuna. **E)** SW edge
 552 of the Tuna travertine mass which is bordered by a m-wide normal fault. **F-F')** Emek cross-section. **G)** Closely-
 553 spaced strike-slip faults in Emek. **H)** Overprinting strike-slip striae on fault infill. **I)** Normal faulting in Emek
 554 Ab. **J)** SW- edge of Emek Ab. where sandstone layers cover the Emek travertine mass. **K)** Precipitation along
 555 fault planes. **L)** Normal faulting in Emek.

556 Slickensides indicate left-lateral faulting. Travertine block rotation inside the fault zones are
 557 exemplified by slickenlines on internal fault slip planes (see grey great circles of slip planes in the
 558 Aydın stereoplot in Fig. 9). Along-strike several fault bifurcations occur. This 600 m long fault zone
 559 can be traced from the upper part of Aydın to the SE end of Sorkun Ab. The NW end of this strike-
 560 slip fault zone can be traced through the landscape as its prolongation forms the transition between the
 561 flat field NE of Sorkun and the steep flank at the foot of the Taşkestik Tepe.

562 Most normal faults in the upper Ballık area are SW-facing towards the graben floor. Between
 563 Aydın and **Upper Tuna**, however, two steeply, NE-dipping normal faults occur (Fig. 9D). Bedding
 564 was tilted to a steep SW-dipping attitude (P207/50) due to small-scale block rotation along these
 565 faults. Mechanical fault striations on polished fault planes indicate pure strike-slip faulting. Two joint
 566 sets are present in Upper Tuna. They are NNE-SSW to NE-SW and NW-SE oriented, congruent to the
 567 two fault populations in this quarry.

568 In **Sorkun**, several short strike-slip faults with a brecciated fault core developed in a flat-pool
 569 travertine facies. Left-lateral fault movement is deduced from slickensides and mineral growth in fault
 570 planes. Joint orientation is very irregular in the Sorkun quarry. The regional NW-SE joint set is still
 571 present, but also other moderately dipping joint sets cut the travertine.

572 In **Sirmersan**, two small travertine bodies are excavated. Bedding often changes internally as
 573 the travertine typically consist of gentle slope-dominated facies. These bodies are covered by a marly
 574 sedimentary unit that continues northwards to the base of the Kepez Tepe. The travertine is cut by rare
 575 strike-slip faults and by one N-facing normal fault with a thick fault infill. NW-SE and E-W joints are
 576 the most abundant.

577 In the **Emek** quarry and in its abandoned part (**Emek Ab.**), travertine dips gently to the NNE
 578 and consists mainly of a flat-pool facies. Faults are consistently parallel and have a steeply SW-
 579 dipping attitude (see stereoplots in Fig. 9). This orientation is also represented by the joint population
 580 in which the majority dips steeply to the SW. The northern part of Emek travertine is cut by three
 581 strike-slip faults (Fig. 9G). The northernmost fault forms the NE excavation front of the quarry and is
 582 filled with a coloured mud rich in iron (brown) and manganese (black) oxi/hydroxides (Fig. 9H).
 583 Gently (L100/20) to moderately ESE-plunging (L130/40) slickenlines, indicative of strike- and
 584 oblique-slip, respectively, overprint steeply-plunging striae (L230/80). Paleosol displacements along
 585 SW-dipping fault planes (P210/80) containing NW-plunging slickenlines (L302/05) indicate a
 586 sinistral strike-slip deformation. In the centre of the active Emek quarry, several parallel, closely-
 587 spaced (20 m spacing) normal faults are present (Fig. 9F-F', G). The largest normal fault is a 3 m-
 588 wide open fault that is filled by mud and travertine blocks and which can be traced along-strike to
 589 Emek Ab. A 20 m normal displacement can be estimated based on the displacement of a thick
 590 paleosol (thick black line in Fig. 9F-F', L) and by dip-slip slickenlines plunging to the SW (L210/55).
 591 Similarly to observations in other quarries, faults had an open nature in which circulating fluids
 592 precipitated as carbonate cements along fault planes (Fig. 9K).

593 **Emek Ab.** is bordered in the SSW by a hectometre-long fault zone. Travertine bedding in the footwall
 594 is gently NNE-dipping. The hangingwall is composed of coarse-grained sandstone layers with a
 595 steeply SSW-dipping attitude (P232/62) (Fig. 9J). This sandstone is situated on a higher
 596 stratigraphical and structural position than the Emek travertine body and represents an interfingering
 597 clastic facies.

598 The 20 m-displacement, normal fault zone crossing the Emek travertine continues towards the
 599 **Lower Tuna** quarry. Here, travertine dips gently to the NNE and marl and mud deposits cover the
 600 hangingwall of this wide fault zone (Fig. 9A-A', E). The northern NE-dipping fault wall (P040/81) is
 601 marked by WNW-plunging slickenlines (L300/48), indicative of normal faulting with a substantial
 602 oblique-slip component.

603

604 *4.6 Strike-reactivated domain in the footwall of Düzçalı fault: the Best Shear Zone, Faber W, Tetik* 605 *and Özçınar quarries*

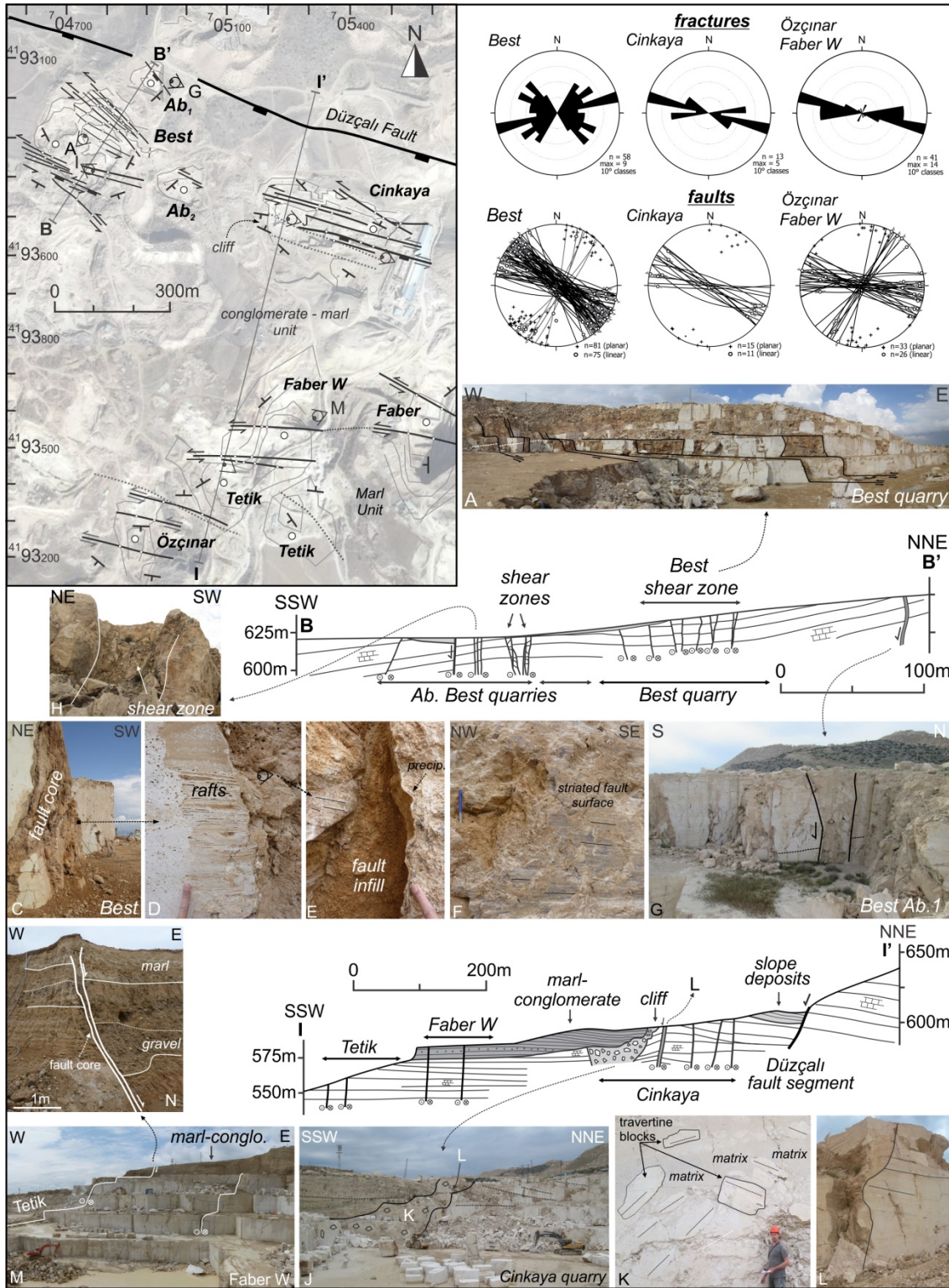
606 In the **Best** quarry and in two adjacent abandoned quarries (Ab₁ and Ab₂ in Fig. 10), travertine dips to
 607 the S, SE and SW and deposition took place along an already developed gentle slope (slope facies.
 608 Numerous parallel, closely-spaced, NW-SE to WNW-ESE-trending strike-slip faults (Fig. 10A, B-B')
 609 can be traced through the Best quarry. Owing to a dense fault spacing, this part of the northern graben
 610 flank is further referred to as the Best Shear Zone. The often metre-thick sedimentary fault infills
 611 consist of brown, chaotically-ordered oxidised muds, small travertine blocks and organic-rich material
 612 (Fig. 10C-E). Successions of paper-thin, brittle, calcite rafts are present in the fault, indicating that
 613 during fault development circulating fluids stagnated for a certain period in the open fault (cf. El
 614 Desouky et al. 2014; Fig. 10D). The fault planes are coated by white to brown calcite cements giving
 615 them a nodular-shaped appearance. Slickenlines and slickensides are mostly only present on the
 616 polished cemented nodule-shaped surfaces and on the muddy fault infill, but never as mechanical
 617 striations on the travertine rock itself (Fig. 10F). Mineral steps on the slickensides all indicate left-
 618 lateral shear suggesting that strike-slip faulting occurred after fluid flow along the fault planes.

619 In the northern part of Best (Fig. 10G), the NW-SE fault orientation deviates from the
 620 dominant WNW-ESE fault orientation found in the entire Ballık area. In this part, also two shear
 621 zones are found (Fig. 10H) in which fault walls are marked by slickenlines and in which the internal
 622 part consists of metre-large rotated travertine blocks. Only two minor normal faults parallel to the
 623 orientation of the adjacent strike-slip faults, are present.

624 Joint sets show a large variety in orientation. Joints are parallel to the WNW-ESE faults, but
 625 also an apparent dominant ENE-WSW joint set is present in the Best quarry. Considering the small
 626 angle (~50°-70°) between both joint sets, they could reflect conjugate jointing during shear
 627 deformation.

628

629



630

631 **Figure 10:** Fault map (basemap © Google Earth) and fault/fracture kinematic analysis (stereoplots) of the
 632 Cinkaya, Best, Faber W, Tetik and Özçınar quarries (NW lower Ballık area). **A)** NW-SE to WNW-ESE strike-
 633 slip faults in the Best quarry. **B-B')** Best shear zone Cross-section . **C)** Shear Zone fault core. **D-F)** Disrupted
 634 muddy fault infill, successions of thin, brittle rafts and cementation/precipitation along the fault wall. Striated
 635 polished nodular-shaped fault wall in **E**. **G-H)** Open faults with infill of travertine blocks. **I-I')** Düzçalı Fault to
 636 Tetik quarry cross-section showing NNE-dipping travertine in Cinkaya and subhorizontal facies in Faber W and
 637 Tetik. Cinkaya travertine is bordered by the Düzçalı fault. **J)** The marl-conglomerate layer (also discussed in
 638 Claes et al., 2015) starts from a cliff (**L**) and covers the travertine of Faber W and Tetik. **K)** Floating travertine
 639 blocks floating in a muddy matrix. **M-N)** Strike slip faults in Tetik and Faber W. continuing through the marl-
 640 conglomerate layer covering the travertine excavated in Faber W.

641 In the **Cinkaya** quarry, bedding is subhorizontal in the middle part, NNE-dipping in the northern part
 642 and SSW-dipping in the SW part of the quarry and deposited as a flat pool facies. Along the western
 643 quarry flank, the SE-dipping travertine mass is abruptly cut by a steep, stepwise erosional cliff (Fig.
 644 10I-I', J, L). A debris layer covers the travertine along the southern edge of this cliff. In this debris
 645 layer, large travertine blocks are irregularly piled up and are 'floating' in a fine-grained travertine
 646 matrix (Fig. 10K). The debris layer can be laterally traced through Cinkaya in a WNW-ESE direction.
 647 Similar cliff-like structures are described along the Honaz fault zone where they are exposed as fault
 648 scarps along major fault segments segments (Koçyiğit, 2005). These similarities suggest that the cliff
 649 in Cinkaya represents an ancient, synsedimentary inactive fault.

650 The Best Shear Zone can be prolonged towards Cinkaya where WNW-ESE strike-slip faults
 651 with left-lateral strike-slip kinematic indicators on the fault infill are observed. On a normal fault in
 652 the centre of Cinkaya, steeply-plunging slickensides are overprinted by subhorizontal slickenlines
 653 indicating that normal faults are strike-slip reactivated. Joints are consistently parallel to the mapped
 654 faults.

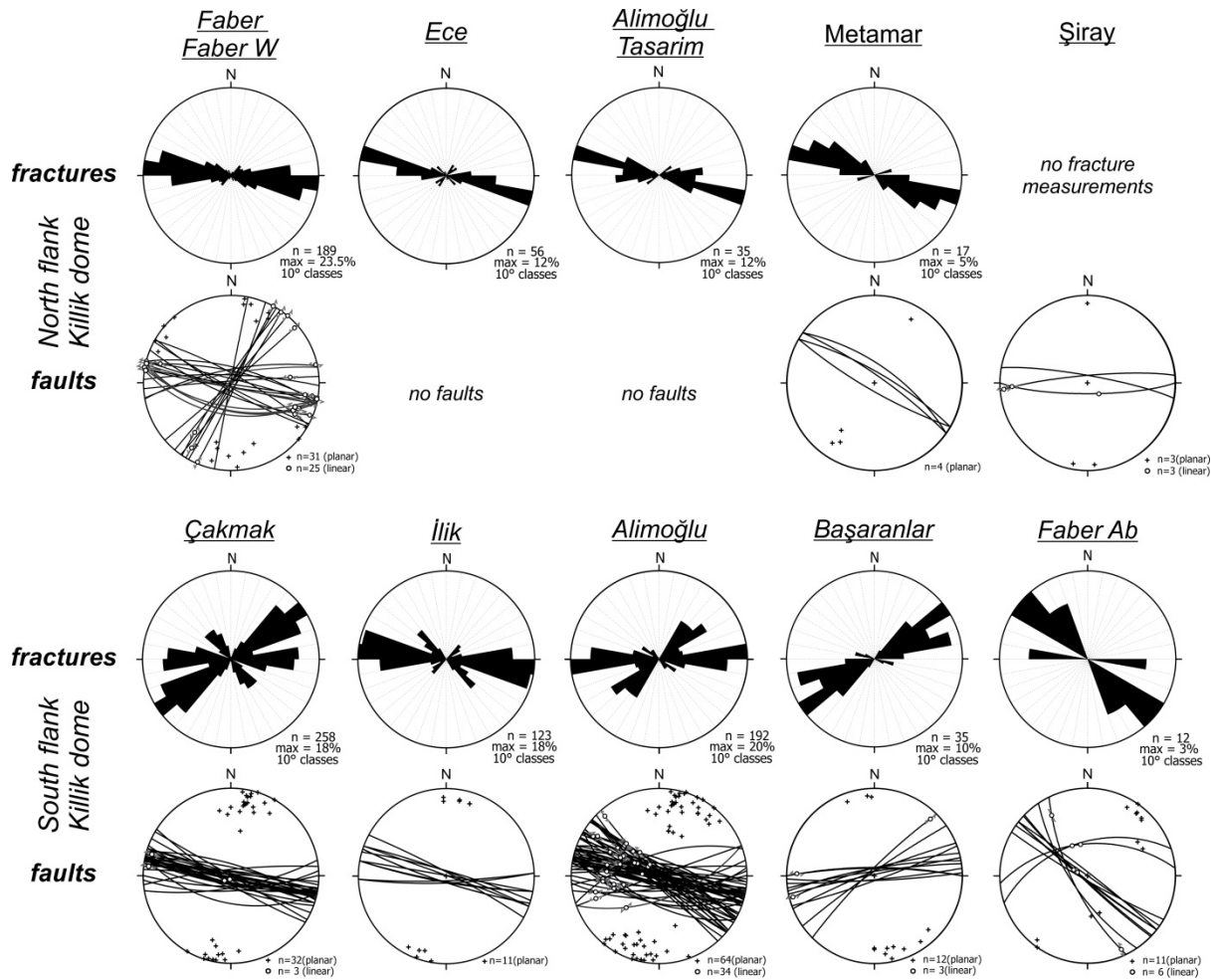
655 The marl-conglomerate alluvial plain unit, of which the debris layer forms the base, continues
 656 to the south, where it reaches a thickness of 20 m. It covers the **Faber W** travertine mass (Fig. 10M)
 657 and thins out to the east in the Faber quarry (i.e. referred to as the marl-conglomerate occurrence in
 658 Claes et al., 2015) where it covers the subhorizontal travertine facies in the lower levels of Faber and
 659 Ece quarries.

660 Joints and faults in **Faber W**, **Tetik** and **Özçınar** show a dominant WNW-ESE orientation
 661 (Fig. 10) and consist of a flat pool facies. Fault walls are marked by subhorizontal E- to W-plunging
 662 subhorizontal slickenlines with sometimes clear left-lateral slickensides. N-S-trending slip planes
 663 often can be observed in the fault infill (see plots of Faber W in Fig. 10). In the sedimentary marl-
 664 conglomerate cover, a normal, northwards-oriented displacement of 2 m has been observed (Fig.
 665 10N). Evidence of post-sedimentary faulting are clay smearing of the incompetent marly layers inside
 666 the fault zone and thickening of a conglomerate layer at the intersection of the fault and the antithetic
 667 fault. Clast rotation (cf. Loveless et al., 2011) cannot be observed due to the fact that clasts are
 668 spherical. Inside the travertine mass, subhorizontal left-lateral strike-slip kinematics are found along
 669 the fault wall of the same fault, indicative of fault reactivation.

670

671 **4.7 Killik domal area and Southern Ballık area**

672 Tectonic deformation and development of the fault/fracture network affecting the Killik domal area
 673 (Faber, Ece, Tetik, Çakmak, İlik, Alimoğlu and Best Ab. Quarries, see Fig. 2) have been extensively
 674 studied by Van Noten et al. (2013). Other researchers have studied the complex sedimentological
 675 build-up of travertine (Özkul et al., 2013; Claes et al., 2015; De Boever et al., 2016; De Boever et al.,
 676 2017) and detritic intervals in these quarries. The Killik dome continues towards the east where it is
 677 excavated by the Alimoğlu Tasarım, Denmer, Başaranlar, Metamar and Şiray quarries.



678

679 **Figure 11:** Fault and fracture orientation analysis (stereoplots) of the Killik dome. See Fig. 2 for quarry
 680 locations. Rose diagrams illustrate fracture distribution. Northern and Southern flanks of the Killik are
 681 separated.
 682

683 Along the northern flank of the Killik dome (**Alimoğlu Tasarım, Metamar**) travertine is
 684 mostly subhorizontal and is covered by a thick marl-conglomerate facies. Alimoğlu Tasarım is
 685 dominated by joints that bifurcate in the cover sediments. In Metamar (Fig. 11), NW-SE normal faults
 686 are parallel to the Düzçalı fault and have NE- and SW displacements, creating a mini-graben in the
 687 Metamar quarry.

688 The travertine in the SW part of the Killik dome (**Çakmak, İlik, Alimoğlu and Best Ab**)
 689 changes from horizontally bedded at the base towards a more complex low-angle slope facies near the
 690 upper part. The eastern domal part (**Denmer, Başaranlar and Şiray**), however, consists of
 691 subhorizontal bedded travertine dipping gently to the SSW and SSE. The fact that the complexity of
 692 the Killik dome does not continue towards the east, suggests that either other major sources may have
 693 been present to cause the formation of the travertine in Denmer and Başaranlar or that these
 694 travertines formed in a later timing and different flow path but from the same spring location. E-W
 695 oriented normal faults cut the edge of the travertine in Başaranlar. In Şiray, faults are also E-W
 696 oriented and show evidence of both normal and strike-slip faulting.

697 Few abandoned quarries (**Faber Ab.**) are present in the area below the cement factory and
 698 north of the Killik fault. Here, a small, NW-SE oriented domal structure, with opposite NE- and SW-
 699 dipping flanks is present. Based on the orientation of this structure and the absence of any connection
 700 with the Killik dome, a different source can be assumed. This travertine mass is cut by several NW-
 701 SE oriented normal faults with subhorizontal slickenlines on the fault infill.

702 Contrary to the tilted blocks along the northern flank of the DGHS, the Killik dome is not
 703 affected by block tilting. Faults have a different orientation along both flanks of the Killik dome.
 704 Whereas NW-SE oriented faults cut the northern flank, E-W to WNW-ESE faults affect the southern
 705 part. This is for instance exemplified by the difference in fault orientation in Şiray and Metamar.
 706 Based on fault distribution, the rigidity of Killik dome thus seems to have played a role in such way
 707 that faults preferentially developed along its flanks after travertine formation but hardly in its centre.
 708 A major fault feeder system responsible for the travertine deposition of the Killik dome has not been
 709 found but based on slope analysis it should be located along the domal axis between the Çakmak - İlik
 710 - Alimoğlu (the southern domal flank) and the Faber – Ece - Alimoğlu Tasarım quarries (the northern
 711 domal flank).

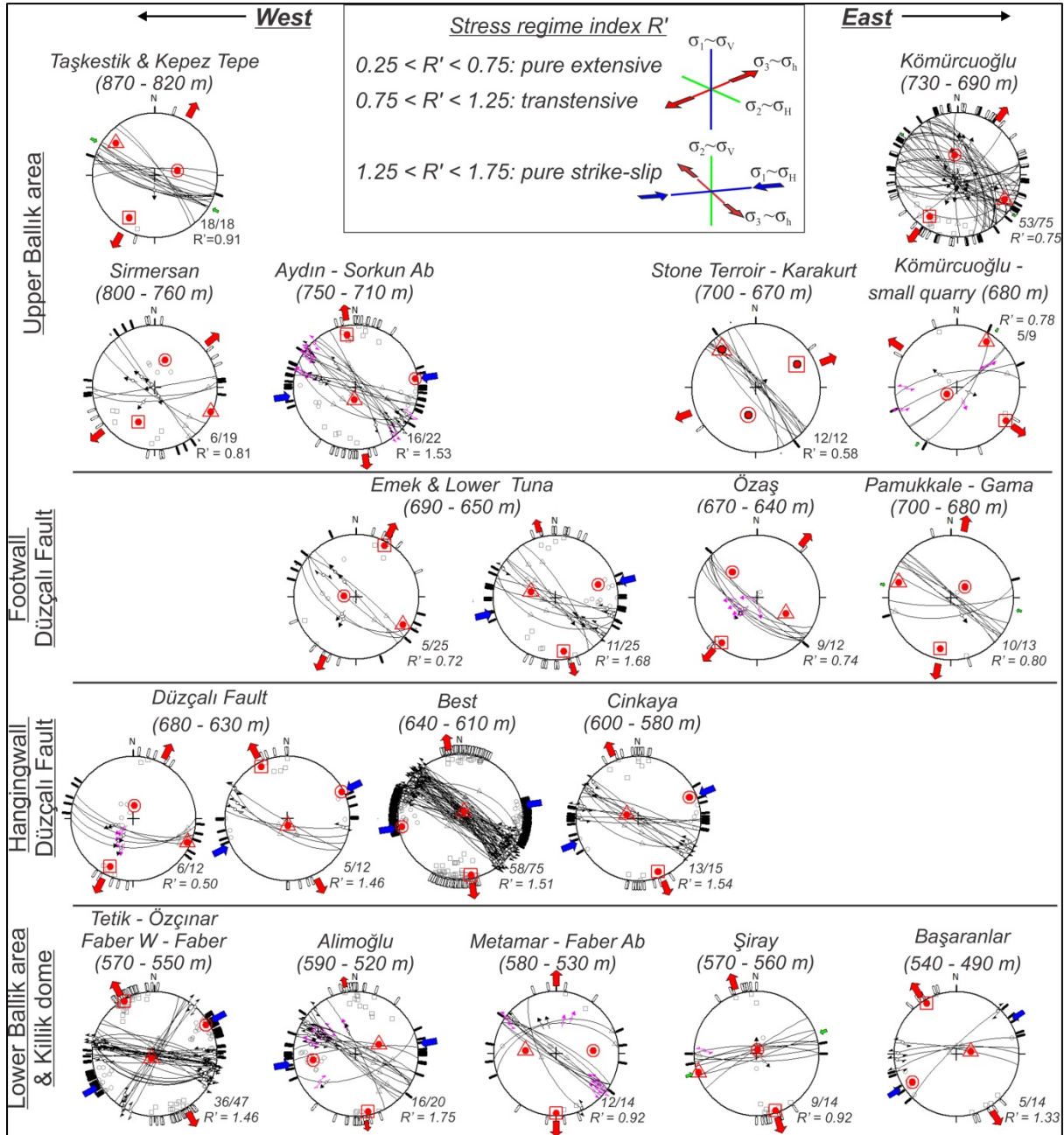
712 In the Killik dome, fracture propagation is influenced by the different travertine facies. Joints
 713 that developed in subhorizontal travertine facies are continuous and straight, whereas joints in slope
 714 facies have an irregular trace and are affected by the local travertine bedding forming staircase
 715 fractures (cf. Maggi et al., 2015). In the northern flank of the Killik dome, i.e. in the NNE-dipping and
 716 subhorizontal flanks, joints are dominant WNW-ESE oriented and are parallel to the mapped normal
 717 and strike-slip faults affecting this part (Fig. 11). As the northern part is situated in the hangingwall of
 718 the Düzçalı fault, joints and faults show a large parallelism to the trace of this fault. In the eastern part
 719 of the Killik dome, i.e. in Çakmak, İlik and Alimoğlu, majority of the joints are parallel to the E-W to
 720 WNW-ESE oriented faults. Two other significant joint sets, i.e. a NW-SE and a NE-SW oriented set,
 721 can be recognised. Towards the eastern end of the Killik dome, joints in Başaranlar are NE-SW
 722 oriented and deviate slightly from the E-W oriented faults. Jointing could here be affected by the
 723 locally NE-SW trending Killik fault. In Faber Ab., fractures are parallel to the local faults and are
 724 dominant NW-SE trending.

725

726 **5. Paleostress analysis**

727 Paleostress inversion results in three orthogonal principal stress axes and the stress ratio $R = (\sigma_2 - \sigma_3) /$
 728 $(\sigma_1 - \sigma_3)$, which classifies the stress tensors as radial/pure/strike-slip extensive,
 729 extensive/pure/compressive strike-slip or strike-slip/pure/radial compressive stress states. Inversion is
 730 sometimes problematic if the observed deformation results from multiphase deformation history and
 731 if fault data is heterogeneous (e.g. Çiftçi and Bozkurt, 2009). To overcome this problem, in this study,
 732 faults observed in different quarries but that have similar kinematics were grouped. To identify

733 different fault populations and stress orientations, we rejected faults with high misfit angles in the
 734 Win_tensor Program until a solution with homogeneous faults was found. When a rejected fault
 735 population resembles faults in neighboring quarries, then this population was regrouped into a new
 736 subset for which the inversion was rerun. The stress regime index R' distinguishes between pure
 737 extensive, transtension and a pure strike-slip regime (Fig. 12).



738
 739 **Figure 12:** Stress inversion of selected fault data and associated slip planes observed in the Ballık area
 740 illustrated in lower-hemisphere equal area stereoplots. Quarries are ordered from west to east in different
 741 domains according to the elevation and tectonic blocks in which they occur. Stress inversion results in the three
 742 principal stress axes (circle for σ_1 , triangle for σ_2 and square for σ_3). Number of used fault-slip data with respect
 743 to the total amount of data for the considered fault data is indicated. Outward arrows indicate extensional
 744 deviatoric stresses; inward arrows represent compressional deviatoric stresses. Blue arrows: σ_1 (S_{Hmax}). Green
 745 arrows: σ_2 (S_{inim}). Red arrows: σ_3 (S_{hmin}). In some quarries (Emek, Lower Tuna, Şiray, Başaranlar and Düzçalı
 746 fault) two stress regimes (NNE-SSW extension and WNW-ESE strike-slip faulting) are deduced. The Düzçalı
 747 fault inversion results from fault data gathered in this study and from Koçyigit (2005).

748

749 Paleostress inversion carried out on the fault data results in two dominant but significantly
 750 different stress regimes: NE-SW pure extension ($R' < 0.75$) to transtension ($0.75 < R' < 1.25$) and a
 751 pure strike-slip regime ($1.25 < R' < 1.75$) with ENE-WSW compression and NNW-SSE extension.
 752 The northeastern (Kömürcüoğlu, Pamukkale, Gama, Stone Terroir, Karakurt) and northwestern
 753 (Kepez and Taşkestik Tepe, Sirmersan) areas were only affected by NE-SW extension to transtension
 754 (= oblique opening). Travertine at the base of the Taşkestik Tepe was strongly affected by the strike-
 755 slip regime.

756 Locally in the small quarry south of Kömürcüoğlu, the deduced NW-SE extension deviates
 757 from regional extension. Because of the local presence of the NE-SW transfer zone between the
 758 Düzçalı and the Elmalı faults in this region (Fig. 2), this NW-SE extension might be a local effect and
 759 cannot be extrapolated to a regional stress regime.

760 Travertine in the footwall of the Düzçalı fault and this fault itself bear characteristics of both
 761 the NE-SW extension regime (Emek, Özaş, Lower Tuna, Pamukkale, Gama, Düzçalı) and the strike-
 762 slip regime (Emek, Emek Ab, Lower Tuna, Düzçalı). Stress inversion of fault data in the lower part of
 763 the Ballık area (Tetik, Özçınar, Faber W, Faber, Alimoğlu, Başaranlar) results in the strike-slip
 764 regime. Strike-slip kinematics are absent in the middle part of the Killik dome (Metamar, Şiray).
 765 Stress inversion shows a slightly different extensional direction with N-S extension.

766 The NE-SW to NNE-SSW extension that deformed the Ballık area clearly shows a
 767 congruence with the current Holocene NE-SW to NNE-SSW extension in the eastern and central parts
 768 of the DGHS, as indicated by focal mechanisms of recent small to moderate earthquakes (Irmak,
 769 2013) and kinematic analysis of the margin-bounding faults along the Denizli and neighbouring
 770 Grabens (Çiftçi and Bozkurt, 2009; Kaypak and Gökaya, 2012).

771

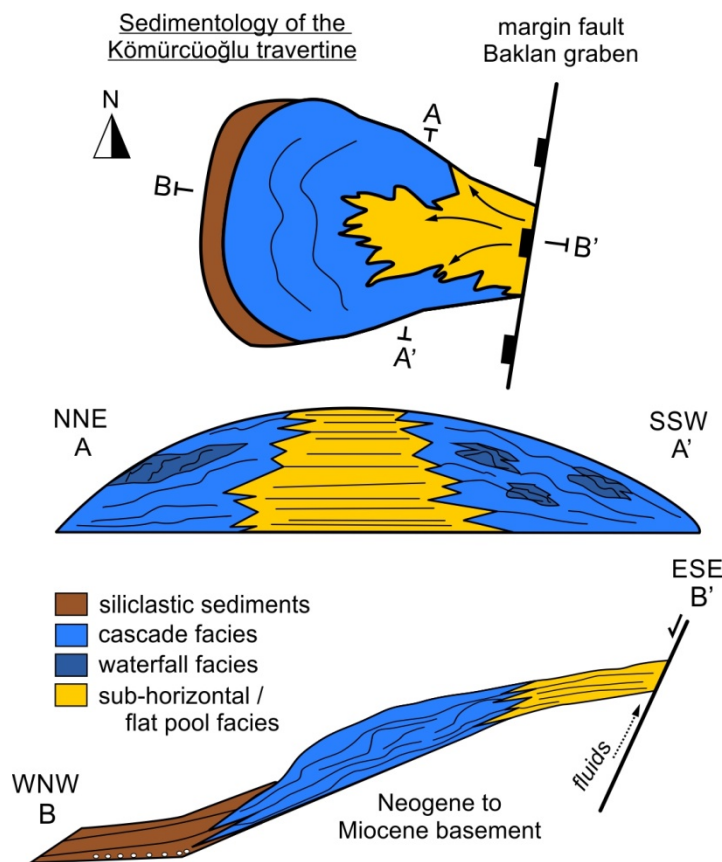
772 **6. Discussion**

773 *6.1 Travertine morphology*

774 Although a detailed travertine facies analysis is beyond the scope of this study, the general dip and
 775 morphology of the different studied travertine deposits can be used to identify the morphology of the
 776 Denizli margin at the time of Pleistocene Ballık travertine deposition and allows tentatively to locate
 777 possible feeder systems. Establishing this morphology is important to separate sedimentological
 778 depositional from tectonic deformation processes. In general, in the Ballık area, travertines occur as
 779 (large) travertine geobodies deposited in flat pools and in slope-controlled travertine mounds in the
 780 eastern part and as individual travertine domes in the western part.

781 The Kömürcüoğlu travertine body (Figs. 2 and 3) is oriented E-W, orthogonal to the
 782 orientation of the nearby travertines in the Ballık area. Based on facies occurrence and present and
 783 deduced paleo-topography, a large mound travertine geobody can be proposed, characterized by a

784 lobe geometry of different facies including subhorizontal, channelled pool terraces (cf. Violante et al.,
 785 1994) and biohermal reed facies (Fig. 13). Based on the oppositely sloping facies a second,
 786 agglomerative lobe was deduced in the SSW part of the K m rc ođlu quarry. The vertical change of
 787 sub-horizontal facies to channelled pool terraces facies (pools and barrages) is related to the increase
 788 in occurrence of higher plants (bryophytes, mosses, reed stems) in the pools. These plants make
 789 barrage bodies and impede water flow, causing changes in topography from East to West at
 790 K m rc ođlu. Higher in stratigraphy biohermal reed facies is formed, eventually leading to a sloping
 791 topography along which rapid water flowed and slope travertine facies developed. The increasing
 792 amount of higher plants (Fig. 5G) towards the top of the deposits represent a cooling and shifting
 793 water flow direction and eventually the formation of paleosol intercalations. Several metre-scale
 794 primary caves develop below hanging plants. Originally, the formation of these hanging plants should
 795 be driven by gravity and should have grown nearly vertically in biohermal reed facies. In southern
 796 K m rc ođlu quarry, however, these plant structures have a steep dip of $\sim 70^\circ$ (Fig. 5G). This
 797 observation indicates that this part of the travertine mass was rotated towards the SE, presumably by
 798 block rotation due to local faulting. At the end of the system travertine deposition ceased, which is
 799 demonstrated by alternation of finer mud sediments and less well-sorted matrix-supported
 800 conglomerates that cover the K m rc ođlu travertine. The detritals are products of cohesive debris
 801 flows (Nemec and Steel, 1984).



802

803 **Figure 13:** Simplified conceptual model and cross-sections of the geometry of the main travertine lobe of the
 804 K m rc ođlu travertine. Based on the lobe geometry, a travertine source WNW of the quarry is expected.

805

806 The paleo-springs as source of the K m rc ođlu mound geobody should be found northeast
807 of the K m rc ođlu quarry. Because the travertine geobody formed in alignment with the NE-SW
808 trending fault system on the front of the fault-controlled Malıdađı mountain (Fig. 1), it is plausible
809 that this fault, which is related to Baklan Graben development, acted as a source. Also north of
810 K m rc ođlu (Fig. 1), the Belevi travertine system developed downslope and was sourced by the NE-
811 SW trending graben-edge fault of the Baklan Graben (Claes et al., 2017b).

812 The travertine in the Killik domal area originated from meteoric fluids that have interacted
813 with basement rocks at depth and emerged along the graben margin faults to the surface (Claes et al.,
814 2015; El Desouky et al., 2015). The Killik dome is a depositional dome with horizontal to
815 subhorizontal bedded travertine present in the lower part that gradually changes upwards to
816 cascade/slope and waterfall facies travertine.

817 Travertine masses developed along the northern graben flank, i.e. the Pamukkale-Gama,
818 Karakurt-Stone Terroir,  zař, Emek-Lower Tuna and Tařkestik-Kepez Tepe travertines consist of
819 WNW-ESE oriented (sub-)horizontal to gently S-wards sloping travertine masses (similar to the
820 ‘eroded-sheet travertines’ of Altunel, 1994). As this subhorizontal travertine facies occurs north
821 (footwall) and south (hangingwall) of the D zçalı fault, a similar large normal fault system should be
822 present at depth north of D zçalı sourcing the necessary fluids for the large-scale observed
823 subhorizontal travertine system . The extent of this fault system is unknown and can be hidden in the
824 underlying Neogene unconsolidated sediments. Hence, sourcing potentially occurred diffuse through
825 these sediments. This interpretation is supported by the fact that no banded travertines or central
826 feeder system has been found in the Ballık area, thus suggesting a large depression as depositional
827 environment (Fig. 14A). The good rock quality of the travertine masses in the upper part suggests that
828 at the time of travertine deposition, already an uplifted mountain morphology must have been present
829 to create subhorizontal to slope-dominated travertine facies that were not totally destroyed by further
830 uplift of the mountain flank.

831 The fact that many siliciclastic sequences intercalate and cover (Fig. 14B) the different
832 travertine masses along the northern margin suggests that a clastic source of sediments must have
833 been located in the mountain range north of the Ballık area (Fig. 1). However, as the Tařkestik Tepe
834 travertine is currently the highest point in the Ballık area, a considerable uplift of the Tařkestik Tepe
835 occurred during the late Pleistocene-Holocene (Fig. 14C) shutting of the Ballık area from this clastic
836 source.

837

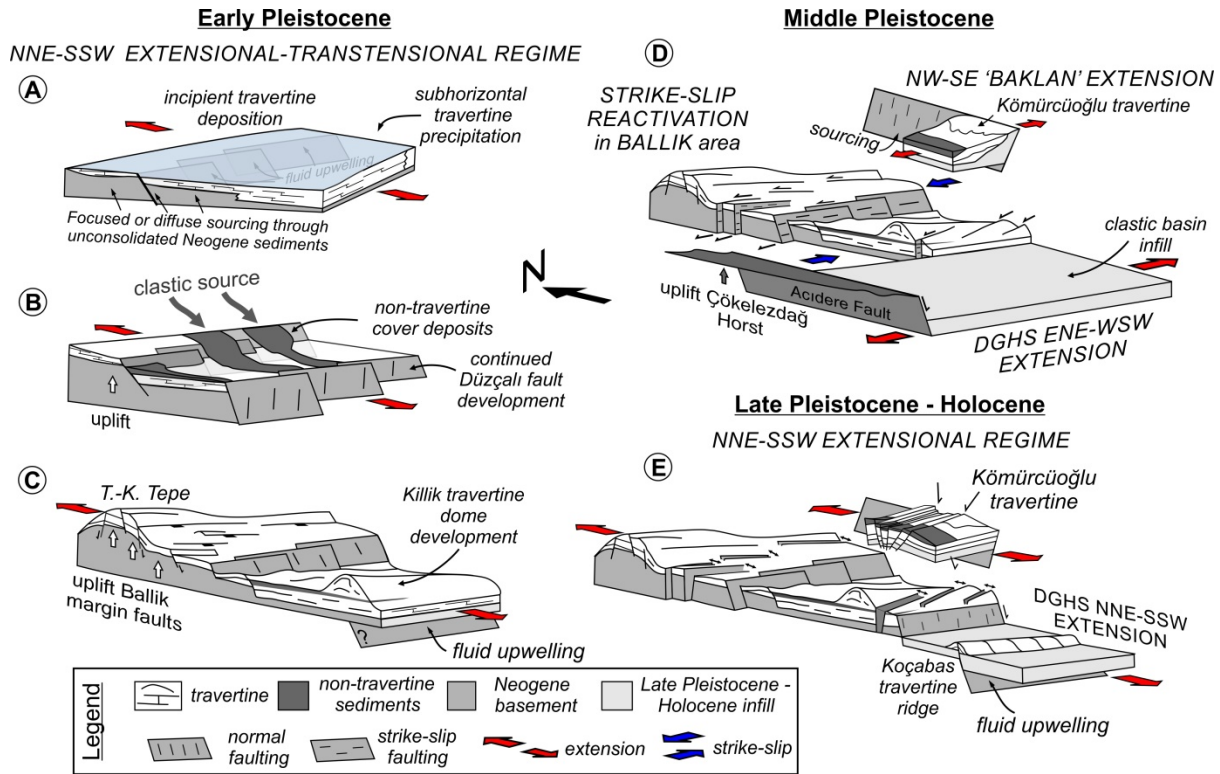


Figure 14: Conclusive cartoon (not to scale) illustrating the sedimentological and tectonic evolution of the Ballık travertine. **A)** Early Pleistocene subhorizontal travertine development on top of Neogene basement sediments/rocks. **B)** Alluvial system covering the travertine with marly and clayey sediments sourced from the mountain range north of the Ballık area. **C)** Normal faulting and uplift of the Taşkestik (T.-K) Tepe simultaneously with development of the Killik travertine dome. **D)** Kömürçüoğlu travertine development, sourced by the NNE-SSW trending Baklan margin fault. Baklan Graben and the DGHS in ENE-WSW extension. Normal faults in the Ballık area reactivated into strike-slip and acting as transfer zone between both regions. **E)** Collapse of the Ballık area with opening and infill of normal faults. Active travertine precipitation occurred further basin-inwards e.g. at Koçabas.

6.2 A relative travertine age model

With limited amount of age data available in literature, restoring a complete chronology of different travertine deposition along the entire northern flank remains enigmatic. However, geomorphological evidence, travertine architecture and fault crossing relationships can be used to constrain a tentative relative travertine age model (Fig. 14). Around the world numerous examples are known (e.g. Turkey, Hungary, off shore Brazil) in which inactive travertines are present at elevated levels, because they were cut off from the main water table due to tectonic uplift, and where active spring travertine precipitation has shifted to lower areas (e.g. González-Martín et al., 1989; Capezzuoli et al., 2010; Özkul et al., 2010; Özkul et al., 2013; Çolak Erol et al., 2015; Claes et al., 2017a; Wang et al., 2017). This also occurred in the DGHS as the Killik dome is younger than the travertine developed along the northern margin flank. Formation of the Killik dome occurred simultaneously when extensional deformation was affecting the already deposited travertine masses along the margin flank (Fig. 14C). Lebatard et al. (2014) concluded from paleomagnetism in combination with cosmogenic nuclide dating that the travertine in the lower part of the Killik dome ranges between 1.7 and 1.1 Ma. The

864 younger, upper parts date between 1.22 and 1.07 Ma (Lebatard et al. 2014) but might have younger
 865 ages as the uppermost levels have not been dated yet. The Taşkestik Tepe lies 260 m higher than the
 866 youngest part of the Killik dome. Taking a general uplift rate of 0.2 mm/a in Anatolia (Westaway et
 867 al., 2003) into account, then the earliest deposition along the Taşkestik Tepe could potentially date
 868 back to 2.5 Ma, i.e. Early Pleistocene (Fig. 14A). This age is probably overestimated as displacement
 869 related to normal faulting is not considered in the calculation and significantly contributed to the
 870 uplift, but it sets an age window in which travertine deposition needs to be framed.

871 U/Th depositional ages of the Kömürçüoğlu and Belevi travertines vary between 490 ± 50 and
 872 510 ± 50 ka (Özkul et al., 2004), which is significantly younger than the Ballık travertine. Because both
 873 travertine masses are sourced from Baklan margin faults, this age suggest that the NE-SW ‘Baklan’
 874 extensional stress regime must have been active during deposition of these travertine masses (Fig.
 875 14D). With time the travertine deposition migrated from the northern graben flank to a more central
 876 part of the DGHS, e.g. at Koçabas (181 ka to 80 ka; Toker et al., 2014) (Fig. 14E).

877

878 ***6.3 Development of the extensional fault/fracture network***

879 In Western Anatolia, the Baklan, Acigöl, Dinar and Burdur Basins are all characterized by master
 880 border faults that progressively young and downthrow towards the depocentre in the basin. The
 881 seismogenic Dinar fault zone (Fig. 1b), for example, is subdivided in an outer and inner fault zone of
 882 which the former is characterised by Miocene-Pliocene strike-slip tectonics, whereas the latter formed
 883 by younger Quaternary normal tectonics (Alçiçek et al., 2013). Also the northern margin of the
 884 Denizli Basin (e.g. at Pamukkale) is characterised by a stepwise basin morphology that is dominated
 885 by normal fault segmentation (Kaypak and Gökkaya, 2012). Travertine formation is mainly associated
 886 to transfer zones between the stepwise NW-trending margin faults (Alçiçek et al., 2015) that also
 887 young towards the basin centre, a process which is accompanied by the development of different
 888 fluvial terraces (Özkul et al., 2013).

889 Also in the Ballık area, faults progressively young from the uplifted horst towards the basin
 890 centre. Hence, the paleostress regimes deduced from the fault kinematica can be used to reconstruct
 891 the deformation of the Ballık area. Because the Quaternary travertines are developed on loose
 892 Neogene sedimentary basin fills, there is a risk that the mapped faults do not resemble the regional
 893 tectonics. Indeed, some suspicious stress inversion results do not resemble the regional inversions but
 894 rather local gravitational collapse (e.g. the NW-SE extension in the Kömürçüoğlu small quarry in Fig.
 895 12 can be linked to activity along the Killik fault). The majority of the stress inversions, however, all
 896 result in very similar stress regimes suggesting that the analysed directions are regional.

897 Similar to the northern graben margin of the Çürüksu Graben, the Ballık area is characterised
 898 by fault segmentation. From the Kepez Tepe quarry in the west to the Pamukkale quarry in the East
 899 the WNW-ESE-oriented travertine masses are not continuous but are rather distributed in an en-
 900 echelon configuration (Fig. 2). This suggests that the underlying blind faults that provide the

901 necessary fluids for travertine precipitation also have such a configuration. Most faults affecting the
 902 subhorizontal to tilted travertine masses are WNW-ESE oriented and are sometimes parallel but
 903 mostly slightly obliquely oriented with respect to the incipient margin-bounding faults such as the
 904 Düzçalı and Killik faults, which show a segmented, en-echelon configuration. The paleostress
 905 inversion of these en-echelon faults indicates that fault segmentation developed during a long-lived,
 906 NNE-SSW oriented extensional-transensional stress regime (Fig. 12, Fig. 14A-C). The dense and
 907 often fault-parallel joint network moreover suggests that faulting was accompanied by fracturing. In
 908 the Kömürcüoğlu quarry, for example, joints and faults in the northern part dip steeply to the south
 909 whereas joints and faults in the southern part dip moderately to the north. This parallelism would not
 910 be present if jointing would post-date faulting.

911 Due to the shallow burial, tensile Mode I fractures dominate the deformation in the Ballık
 912 area. The alignment and consistent orientation of joints and extension veins contribute to the
 913 interpretation of the paleostress results as Mode I fractures open perpendicular to minimum principal
 914 stress direction (σ_3), both at shallow (Laubach et al., 2004) or at large depths (Van Noten et al., 2012).
 915 As close to the Earth's surface differential stresses are low (Hancock and Engelder, 1989), differences
 916 in principal stress magnitudes are small and consequently stress permutations, in which σ_1 , σ_2 and σ_3
 917 can shortly swap, may occur. Based on these arguments, Van Noten et al. (2013) concluded that the
 918 three dominant joint sets in the Killik dome result from stress permutations in the Pleistocene
 919 resulting from NNE-SSW and E-W extension induced by the DGHS Graben and by NW-SE
 920 extension from the Baklan Graben (further noted as 'Baklan' extension). Also in the western part of
 921 the DGHS, different joint sets observed in fissure ridges reflect multiple extension directions of
 922 adjacent basins (Altunel and Hancock, 1993a; Altunel and Karabacak, 2005).

923

924 **6.4 Strike-slip tectonics**

925 The muddy fault infill and the secondary cementation phases are often striated by subhorizontal
 926 slickenlines which are interpreted as strike-slip reactivation features. The strike-slip tectonic stress
 927 regime that caused this reactivation clearly post-dates the NNE-SSW extensional phase as strike-slip
 928 markers are always observed on normal fault infills and hardly ever as mechanical striations directly
 929 on fault walls.

930 Stress inversion of the Ballık strike-slip fault reactivation data results in an ENE-WSW
 931 oriented σ_1 (compression) and NNW-SSE oriented σ_3 (extension) (Fig. 12). This orientation is the
 932 proper orientation to activate the NNE-SSW Baklan margin faults. The similarity in orientation of σ_3
 933 during 'Baklan' extension with σ_1 in the strike-slip regime of the Ballık area strongly suggests that
 934 'Baklan' extension can be interpreted as the reactivation force of the ENE-WSW fault network in the
 935 Ballık area. When NW-SE 'Baklan' extension affected the DGHS, the NNE-trending Acidere fault
 936 east of the Ballık area (Figs. 2 and 17) was favourably oriented to be also reactivated as an oblique
 937 normal fault (Koçyiğit, 2005) causing subsidence of the Denizli basin floor and uplift of the footwall,

938 i.e. giving rise to the Çökelezdağ Horst (Fig. 14D). To reach this particular stress configuration, σ_2
 939 and σ_3 in the DGHS switched to change from regional NNE-SSW Denizli extension to regional NW-
 940 SE to WNW-ESE ‘Baklan’ extension.

941 In a fault network, faults tend to involve reactivation of existing faults rather than creating
 942 new faults (Scholz, 1998), especially if the fault orientation is in an optimum angle for reactivation
 943 (Sibson, 1985). At the time when ‘Baklan’ extension affected the Acidere fault, the inherited WNW-
 944 ESE Ballık fault network thus acted as border faults for this extension and was, given its favourable
 945 orientation, reactivated into sinistral strike-slip faults. The Ballık area can thus be considered as a
 946 strike-slip transfer zone from the Acidere fault to the western border fault of the Baklan basin.

947 The K m rc ođlu, Gama and Pamukkale travertine masses are preserved from strike-slip
 948 faulting. They are situated at the southern end of the Baklan Graben and are thus excluded from the
 949 transfer zone and hence neither strike-slip faults or any NE-SW trending joints affected these quarries.
 950 Also along the Kepez and Tařkestik Tepe, no strike-slip features are observed as these travertine
 951 masses were already uplifted along the margin shoulders and the limited length of the Acidere fault to
 952 the north.

953 Another argument of graben interaction was given by Kaymakçı (2006) who modelled the
 954 stress magnitudes in the DGHS. He proved that sharp changes occur around subsurface lineaments at
 955 places where major basin geometrical changes occur. The change in basin geometry from E to W
 956 orientation between G rleyik and Honaz to a NW to SE orientation between Kocabař and Ballık (Fig.
 957 2) shows that the NW-SE extension of the neighbouring Baklan Graben strongly contributed to the
 958 evolution of the eastern DGHS.

959 With exception of the Ballık area, large-scale strike-slip faulting has hardly ever been
 960 observed in the DGHS. The only mappable strike-slip faults are two closely-spaced faults affecting
 961 the Upper Miocene ancient basin fill in the Alikurt area in the easternmost Kaklık area (see the
 962 opposite facing-faults at Alikurt in the eastern part of Fig. 2) (Koçyiđit, 2005) and a NW-trending
 963 strike-slip fault at Hierapolis offsetting an historic man-made channel (Altunel and Hancock, 1993b).
 964 Kinematic analysis of overprinting slickensides on the former example indicates that a strike-slip
 965 regime with ENE-WSW compression has taken place at the end of the Middle Pliocene in the Alikurt
 966 area, post-dating an earlier regional NNE-SSW extension phase (Koçyiđit, 2005), quite similar to the
 967 tectonic evolution of the Ballık area. This Middle Pliocene phase of strike-slip predates Ballık
 968 travertine precipitation but indicates that during the development of the DGHS transient periods of
 969 regional stress reconfigurations have taken place at its borders showing tectonic influences of adjacent
 970 basins.

971 Similar stress reconfigurations driving fault reactivation are also recognised along the NW
 972 margin faults of the Baklan Graben. The Baklan, Acig l and Burdur halfgrabens are all three bounded
 973 by major NW-dipping normal faults and are considered to have initiated parallel to the Dinar transfer
 974 zone during the late Miocene-Pliocene in a NW-SE oriented extensional phase (Westaway, 1990).

975 Further development and NE-SW opening of the Dinar Basin in the Quaternary resulted in sinistral
 976 oblique-slip reactivation of the NW-normal faults bounding the Baklan, Acigöl and Burdur Basins,
 977 due to differential stretching of the inner blocks on top of the Dinar fault zone (Westaway, 1990;
 978 Sintubin et al., 2003; Verhaert et al., 2006; Gürbüz et al., 2012; Alçıçek et al., 2013).

979

980 **6.5 Late Pleistocene – Holocene extension**

981 During the late Pleistocene – Holocene considerable block tilting has taken place. The NNE-dipping
 982 travertine observed in the Reisoğlu-Özaş, Emek, Lower Tuna, Kepez and Taşkestik Tepe and Cinkaya
 983 quarries (Figs. 7, 8, 9 and 10) are examples of block tilting as travertine in the hangingwall is tilted
 984 northwards towards the footwall as a result of normal faulting. Another example of block tilting
 985 occurs in the southern part of the Emek, Kepez and Taşkestik Tepe quarries where travertine in the
 986 hangingwall of normal faults dips towards the Denizli Basin to the SSW (Figs. 7C-C' and 11F-F').

987 Many faults along the northern flank are filled by clayey and marly sediments, either by
 988 gravitational or hydrological transport, and calcite cementation along the fault walls is common. The
 989 sedimentary infill, open nature of the faults, various fracture patterns and dissolution-enlarged
 990 fractures are typical for shallow dilatant fault zones developed along already uplifted extensional
 991 graben shoulders (van Ghendt et al., 2010). Fault widening and infill is observed along both strike-slip
 992 reactivated and normal faults and can be related to this late deformation stage (Fig. 14E).

993 The fact that the Killik fault delimits the Killik dome and cuts all faults affecting the Killik
 994 dome, suggests that the latest activity in Ballık area took place along the Killik fault. After all, alluvial
 995 Quaternary sediments are deposited in the Denizli basin floor in the hangingwall of the Killik fault.
 996 The left-lateral stepwise orientation of the Killik fault moreover suggests that a transtensional
 997 component was still present in the late-Pleistocene to Holocene causing further oblique opening in
 998 this part of the DGHS. Active extension and related travertine precipitation took place further basin
 999 inwards illustrated by several travertine ridges at e.g. Kocabaş.

1000 Focal mechanisms of recent earthquakes (Taymaz and Price, 1992; Price and Scott, 1994;
 1001 Gürbüz et al., 2012; Kaypak and Gökçaya, 2012; Irmak, 2013), geodetic data, southwestwards GPS-
 1002 based vectors (Elitez and Yalıtırak, 2016) and stress indicators on the World Stress Map (e.g. N23E
 1003 extension for the M_L 4.8 20080425 earthquake at Gürleyik, Fig. 1) all indicate that current extension
 1004 is still NNE-SSW in the eastern DGHS.

1005

1006 **7. Conclusions**

1007 A detailed structural mapping of neotectonic faults and fractures and a tentative evaluation of the
 1008 Ballık travertine geodynamic evolution lead to a reconstruction of the kinematic deformation history
 1009 of the eastern part of the Denizli Graben-Horst System in SW Turkey. This study demonstrates the
 1010 importance of incorporating tectonic fault analyses into travertine geobody reconstructions to

1011 understand the geodynamic history of continental carbonates. Based on the detailed tectonic analysis
 1012 and paleostress inversion carried out on fault-slip data gathered from 35 quarries, the following
 1013 conclusions can be drawn:

- 1014 1) As one of the best tectonically characterized reservoir-scale travertines, the Ballık travertine
 1015 forms the ideal base for reservoir modelling with integration of sedimentological and tectonic
 1016 data from μm to seismic-scale.
- 1017 2) The Ballık travertine is deformed by WNW-ESE-oriented normal faults that are either parallel or
 1018 slightly oblique to the Düzçalı and Killik incipient margin-bounding faults. The upper part of the
 1019 margin was only affected by extension and is marked by backtilted travertine in the hangingwall
 1020 of normal faults. In the foot- and hangingwall of the Düzçalı fault and in the lower Killik dome,
 1021 WNW-ESE normal faults are reactivated into sinistral strike-slip faults. Reactivation is
 1022 evidenced by strike-slip slickenlines that are mostly developed on the muddy fault infill and on
 1023 polished surfaces of secondary cement infill.
- 1024 3) Paleostress inversion results in two dominant paleostress regimes. Travertine precipitation and
 1025 subsequent emplacement of the fault network took place during a long-lived phase of NNE-SSW
 1026 extension in the early Pleistocene. Block tilting, back rotation, fault infill, secondary fluid flow
 1027 and extensional fracturing, creating a dense joint network, accompanied faulting during this
 1028 stress state. The sinistral reactivation of normal faults corresponds to a strike-slip regime with
 1029 NE-SW to ENE-WSW compression and NW-SE to NNW-SSE extension in the Ballık area. This
 1030 phase can be related to a NW-SE extensional stress-state during which the NNE-SSW border
 1031 faults of the Baklan Graben were in extension and during which the edge of the eastern part of
 1032 the DGHS, i.e. the Acidere fault, was favourably oriented to be reactivated. The Ballık area acted
 1033 as a transfer zone in this period. A NNE-SSW extensional phase reinstalled in the late
 1034 Pleistocene-Holocene causing further fault widening in the Ballık area and active travertine
 1035 deposition in the central part of the DGHS. This stress state is currently still active.
- 1036 4) Large travertine deposits are likely to found at graben intersections because of the presence of an
 1037 underground fault-fracture network that can be formed during different tectonic regimes. Graben
 1038 intersections are therefore susceptible to an enhanced fluid flow induced by stress permutations
 1039 and fault reactivation.
- 1040 5) Based on fault distribution of the Killik dome it is concluded that large domes have a large
 1041 rigidity with fault development affecting preferentially its flanks but hardly its centre.
- 1042 6) Faults developed at the intersection of different extensional graben structures can easily
 1043 reactivate due to stress reconfigurations, whereas this is less common in the middle of such
 1044 grabens.

1045

1046 **Acknowledgements**

1047 The authors would like to thank the numerous quarry owners, workers and engineers in the Ballık area
 1048 for their kind hospitality, logistic help and interest during field work. This work was undertaken in a
 1049 collaboration between KU Leuven, Pamukkale University and the Royal Observatory of Belgium
 1050 during the TraRAS (Joint Industry Project) research project focusing on the architecture of travertine
 1051 geobodies as reservoir analogue. Marcelle Marques Erthal, Eva De Boever, Jeroen Soete, Michaël
 1052 Verbiest, Klaus Gessner and an anonymous reviewer are thanked for discussion on the early version
 1053 of the manuscript. We are grateful to Total, Petrobras and Shell for partial funding.

1054
 1055 **Online Supplementary data**

1056 **S1:** Google Earth™ Kml-file (cf. Fig. 2) presenting all fault and travertine characteristics discussed in
 1057 this study. All geomorphological faults surrounding the Ballık area are indicated. Yellow dots
 1058 indicate the location of the different quarries. Yellow dots are fault observation points. Faults are
 1059 mapped by connecting individual fault observations. Bedding orientation is indicated by coloured
 1060 areas and correspond to bedding in Fig. 2: Green areas: S-dipping travertine; Purple: N-dipping
 1061 travertine; Yellow areas: W-dipping travertine; Brown areas: Marl, sandstone or conglomerate cover
 1062 deposits; Blue areas: subhorizontal travertine; Blue axis: travertine domal axis..

1063
 1064 **S2:** Quarry location information and fault type info. Quarries in the table are organised in same order
 1065 as they are described in the text. **NF** = normal faulting, **SS** = newly-formed strike-slip faults, **SS r.** =
 1066 reactivated normal faults with strike-slip kinematics. Non-georeferenced fault and fracture orientation
 1067 data measured in each quarry is provided for reproducibility. Type (of measurement): Plane (P)
 1068 orientation noted in dip direction (dd)/dip (d); Lineation (L) noted in in trend (tr) / plunge (pl). A
 1069 lineation following a plane is the lineation measured on that plane. See kml and Fig. 2 for location of
 1070 the quarries.

1071
 1072 **References**

1073 Alçiçek, C., Brogi, A., Capezzuoli, E., Gandin, A., Liotta, D., Meccheri, M., Ruggieri, G., 2015. Extensional
 1074 structures and hydrothermal fluid flow in Western Anatolia: a review from the Neogene-Quaternary Dinar
 1075 and Denizli Basins. *Acta Volcanologica* **26(1-2)**--**27(1-2)**, 123-135.
 1076 Alçiçek, H., Varol, B., Özkul, M., 2007. Sedimentary facies, depositional environments and palaeogeographic
 1077 evolution of the Neogene Denizli Basin, SW Anatolia, Turkey. *Sedimentary Geology* **202(4)**, 596-637.
 1078 Alçiçek, M.C., Brogi, A., Capezzuoli, E., Liotta, D., Meccheri, M., 2013. Superimposed basin formation during
 1079 Neogene–Quaternary extensional tectonics in SW-Anatolia (Turkey): Insights from the kinematics of the
 1080 Dinar Fault Zone. *Tectonophysics* **608**, 713-727.
 1081 Altunel, E., 1994. Active tectonics and the evolution of Quaternary travertines at Pamukkale, Western Turkey.
 1082 PhD thesis, University of Bristol, pp 236.
 1083 Altunel, E., 2000. Historical earthquake activity in and around Hierapolis. In: D’Andria, F., Silvestrelli, F.
 1084 (Eds.), *Ricerche Archeologiche Turche Nella Valle Del Lykos, Lykos Vadisi Turk Arkeoloji Arastirmalari*.
 1085 Congedo Editore. (in Italian and Turkish). p. 299-325
 1086 Altunel, E., Hancock, P.L., 1993a. Active fissuring and faulting in Quaternary travertines at Pamukkale, western
 1087 Turkey. *Z Geomorph NF* **94**, 285 - 302.

- 1088 Altunel, E., Hancock, P.L., 1993b. Morphology and structural setting of Quaternary travertines at Pamukkale,
1089 western Turkey. *Geological Journal* **28**, 335-346.
- 1090 Altunel, E., Hancock, P.L., 1996. Structural Attributes of Travertine-Filled Extensional Fissures in the
1091 Pamukkale Plateau, Western Turkey. *International Geology Review* **38**(8), 768-777.
- 1092 Altunel, E., Karabacak, V., 2005. Determination of horizontal extension from fissure-ridge travertines: a case
1093 study from the Denizli Basin, southwestern Turkey. *Geodinamica Acta* **18**(3-4), 333-342.
- 1094 Angelier, J., Mechler, P., 1977. Sur une méthode graphique de recherche des contraintes principales également
1095 utilisable en tectonique et en séismologie: la méthode des dièdres droits. *Bulletin de la Société géologique de*
1096 *France* **(7)19**(6), 1309-1318.
- 1097 Bott, M.P.H., 1959. The mechanics of oblique-slip faulting. *Geological Magazine* **96**, 109–117.
- 1098 Bozkurt, E., 2001. Neotectonics of Turkey - a synthesis. *Geodinamica Acta* **14**, 3-30.
- 1099 Bozkurt, E., Sözbilir, H., 2006. Evolution of the Large-scale Active Manisa Fault, Southwest Turkey:
1100 Implications on Fault Development and Regional Tectonics. *Geodinamica Acta* **19**(6), 427-453.
- 1101 Brogi, A., 2004. Faults linkage, damage rocks and hydrothermal fluid circulation: Tectonic interpretation of the
1102 Rapolano Terme travertines (southern Tuscany, Italy) in the context of Northern Apennines Neogene–
1103 Quaternary extension. *Eclogae geol. Helv.* **97**, 307-320.
- 1104 Brogi, A., Capezzuoli, E., 2009. Travertine deposition and faulting: the fault-related travertine fissure-ridge at
1105 Terme S. Giovanni, Rapolano Terme (Italy). *International Journal of Earth Sciences* **98**, 931-947.
- 1106 Brogi, A., Capezzuoli, E., 2014. Earthquake impact on fissure-ridge type travertine deposition. *Geological*
1107 *Magazine. Rapid Communication*, 1-9.
- 1108 Brogi, A., Capezzuoli, E., Alçiçek, M.C., Gandin, A., 2014. Evolution of a fault-controlled fissure-ridge type
1109 travertine deposit in the western Anatolia extensional province: the Çukurbağ fissure-ridge (Pamukkale,
1110 Turkey). *Journal of the Geological Society*.
- 1111 Brogi, A., Capezzuoli, E., Aqué, R., Branca, M., Voltarrio, M., 2010. Studying travertine for neotectonic
1112 investigations: Middle-Late Pleistocene syn-tectonic travertine deposition at Serra di Rapolano (Northern
1113 Apennines, Italy). *International Journal of Earth Sciences* **99**, 1383-1398.
- 1114 Brogi, A., Capezzuoli, E., Buracchi, E., Branca, M., 2012. Tectonic control on travertine and calcareous tufa
1115 deposition in a low-temperature geothermal system (Sarteano, Central Italy). *Journal of the Geological*
1116 *Society* **169**(4), 461-476.
- 1117 Buckley, J.P., Elders, C., Mann, J., 2013. Carbonate Buildups in the Santos Basin, Offshore Brazil. *Programme*
1118 *and Abstract Volume: Microbial Carbonates in Space and Time: Implications for Global Exploration and*
1119 *Production. The Geological Society. 19–20 June, 2013.*
- 1120 Çakır, Z., 1999. Along-strike discontinuities of active normal faults and its influence on Quaternary travertine
1121 deposition; examples from western Turkey, Turkish Journal of Earth Sciences, 8, 67-80. *Turkish Journal of*
1122 *Earth Sciences* **8**, 67-80.
- 1123 Capezzuoli, E., Gandin, A., Sandrelli, F., 2010. Calcareous tufa as indicators of climatic variability: a case study
1124 from southern Tuscany (Italy). *Geological Society, London, Special Publications* **336**(1), 263-281.
- 1125 Çelik, S., Çobanoğlu, İ., Atatanır, L., 2014. General material properties of Denizli (SW Turkey) travertines as a
1126 building stone. *Bulletin of Engineering Geology and the Environment* **73**(3), 825-838.
- 1127 Çiftçi, N.B., Bozkurt, E., 2009. Pattern of normal faulting in the Gediz Graben, SW Turkey. *Tectonophysics*
1128 **473**(1–2), 234-260.
- 1129 Claes, H., Degros, M., Soete, J., Claes, S., Kele, S., Mindszenty, A., Török, Á., El Desouky, H., Vanhaecke, F.,
1130 Swennen, R., 2017a. Geobody architecture, genesis and petrophysical characteristics of the Budakalász
1131 travertines, Buda Hills (Hungary). *Quaternary International* **437**, 107-128.
- 1132 Claes, H., Erthal, M., Soete, J., Özkul, M., Swennen, R., 2017b. Shrub and pore type classification: Petrography
1133 of travertine shrubs from the Ballık-Belevi area (Denizli, SW Turkey). *Quaternary International* **437**, 147–
1134 163.
- 1135 Claes, H., Soete, J., Van Noten, K., El Desouky, H., Marques Erthal, M., Vanhaecke, F., Özkul, M., Swennen,
1136 R., 2015. Sedimentology, three-dimensional geobody reconstruction and carbon dioxide origin of
1137 Pleistocene travertine deposits in the Ballık area (south-west Turkey). *Sedimentology* **62**, 1408-1445.
- 1138 Çobanoğlu, I., Çelik, S.B., 2012. Determination of strength parameters and quality assessment of Denizli
1139 travertines (SW Turkey). *Engineering Geology* **129-130**, 38-47.
- 1140 Çolak Erol, S., Özkul, M., Aksoy, E., Kele, S., Ghaleb, B., 2015. Travertine occurrences along major strike-slip
1141 fault zones: Structural, depositional and geochemical constraints from the Eastern Anatolian fault System
1142 (EAFS), Turkey. *Geodinamica Acta*, DOI: 10.1080/09853111.2014.979530.
- 1143 De Boever, E., Foubert, A., Lopez, B., Swennen, R., Jaworowski, C., Özkul, M., Virgone, A., 2017.
1144 Comparative study of the Pleistocene Cakmak quarry (Denizli Basin, Turkey) and modern Mammoth Hot
1145 Springs deposits (Yellowstone National Park, USA). *Quaternary International* **437**, 129-146.

- 1146 De Boever, E., Foubert, A., Oligschlaeger, D., Claes, S., Soete, J., Bertier, P., Özkul, M., Virgone, A., Swennen,
1147 R., 2016. Multiscale approach to (micro)porosity quantification in continental spring carbonate facies: Case
1148 study from the Cakmak quarry (Denizli, Turkey). *Geochemistry, Geophysics, Geosystems* **17**(7), 2922-2939.
- 1149 De Filippis, L., Billi, A., 2012. Morphotectonics of fissure ridge travertines from geothermal areas of Mammoth
1150 Hot Springs (Wyoming) and Bridgeport (California). *Tectonophysics* **548-549**, 34-48.
- 1151 De Filippis, L., Faccenna, C., Billi, A., Anzalone, E., Brillì, M., Özkul, M., Soligo, M., Tuccimei, P., Villa, I.M.,
1152 2012. Growth of fissure ridge travertines from geothermal springs of Denizli Basin, western Turkey.
1153 *Geological Society of America Bulletin* **124**, 1629-1645.
- 1154 De Filippis, L., Faccenna, C., Billi, A., Anzalone, E., Brillì, M., Soligo, M., Tuccimei, P., 2013. Plateau versus
1155 fissure ridge travertines from Quaternary geothermal springs of Italy and Turkey: Interactions and feedbacks
1156 between fluid discharge, paleoclimate, and tectonics. *Earth-Science Reviews* **123**(0), 35-52.
- 1157 Delvaux, D., Sperner, B., 2003. Stress tensor inversion from fault kinematic indicators and focal mechanism
1158 data: the TENSOR program. In: Nieuwland, D. (Eds.), *New Insights into Structural Interpretation and*
1159 *Modelling*. Geological Society, London, Special Publications, 212: 75-100.
- 1160 El Desouky, H., Soete, J., Claes, H., Özkul, M., Vanhaecke, F., Swennen, R., 2015. Novel applications of fluid
1161 inclusions and isotope geochemistry in unravelling the genesis of fossil travertine systems. *Sedimentology*
1162 **62**(1), 27-56.
- 1163 Elitez, İ., Yaltrak, C., 2016. Miocene to Quaternary tectonostratigraphic evolution of the middle section of the
1164 Burdur-Fethiye Shear Zone, south-western Turkey: Implications for the wide inter-plate shear zones.
1165 *Tectonophysics* **690**, 336-354.
- 1166 Faccenna, C., 1994. Structural and hydrogeological features of Pleistocene shear zones in the area of Rome
1167 (Central Italy). *Annali di Geofisica* **37**(1), 121-133.
- 1168 Faccenna, C., Soligo, M., Billi, A., De Filippis, L., Funicello, R., Rossetti, C., Tuccimei, P., 2008. Late
1169 Pleistocene depositional cycles of the Lapis Tiburtinus travertine (Tivoli, Central Italy): Possible influence
1170 of climate and fault activity. *Global and Planetary Change* **63**(4), 299-308.
- 1171 Gessner, K., Gallardo, L.A., Markwitz, V., Ring, U., Thomson, S.N., 2013. What caused the denudation of the
1172 Menderes Massif: Review of crustal evolution, lithosphere structure, and dynamic topography in southwest
1173 Turkey. *Gondwana Research* **24**(1), 243-274.
- 1174 González-Martín, J.A., García del Cura, M.A., Ordóñez, S., 1989. Formaciones tobaceas en los valles Tajuña y
1175 Tajo. In: *Excursion Guide C-4. Reunion del Cuaternario Iberico, Madrid 25-29 September 1989.*
1176 *Association of Española Estudio del Cuaternario (AEQUA) – Grupo Trabalho Portugies Estudodo*
1177 *Quaternario (GTPEQ)*.
- 1178 Guo, L., Riding, R., 1998. Hot-spring travertine facies and sequences, Late Pleistocene, Rapolano Terme, Italy.
1179 *Sedimentology* **45**, 163-180.
- 1180 Gürbüz, A., Boyraz, S., Ismael, M.T., 2012. Plio-Quaternary development of the Baklan–Dinar graben:
1181 implications for cross-graben formation in SW Turkey. *International Geology Review* **54**(1), 33-50.
- 1182 Hancock, P.L., Chalmers, R.M.L., Altunel, E., Çakir, Z., 1999. Travitronics: using travertines in active fault
1183 studies. *Journal of Structural Geology* **21**, 903-916.
- 1184 Hancock, P.L., Engelder, T., 1989. Neotectonic joints. *Geological Society of America Bulletin* **101**(10), 1197-
1185 1208.
- 1186 Irmak, S., 2013. Focal mechanisms of small-moderate earthquakes in Denizli Graben (SW Turkey). *Earth*
1187 *Planets Space* **65**, 943-955.
- 1188 Irmak, S., Taymaz, T., 2009. Source Mechanics of Recent Moderate Earthquakes Occurred in Honaz-Denizli
1189 (W Turkey) Graben Obtained by Regional Broadband Waveform Inversion. In: *International Symposium on*
1190 *Historical Earthquakes and Conservation of Monuments in the Eastern Mediterranean Region*, Istanbul,
1191 Turkey, 350-356.
- 1192 Kaymakçı, N., 2006. Kinematic development and paleostress analysis of Denizli Basin (W Turkey):
1193 implications of spatial variation of relative paleostress magnitudes and orientations. *Journal of Asian Earth*
1194 *Sciences* **27**, 207-222.
- 1195 Kaypak, B., Gökkaya, G., 2012. 3-D imaging of the upper crust beneath the Denizli geothermal region by local
1196 earthquake tomography, western Turkey. *Journal of Volcanology and Geothermal Research* **211-212**, 47-
1197 60.
- 1198 Kele, S., Demény, A., Siklósy, Z., Németh, T., Tóth, M., Kovács, M.B., 2008. Chemical and stable isotope
1199 composition of recent hot-water travertines and associated thermal waters, from Egerszalók, Hungary:
1200 Depositional facies and non-equilibrium fractionation. *Sedimentary Geology* **211**(3-4), 53-72.
- 1201 Kele, S., Özkul, M., Főrizs, I., Gőkgőz, A., Baykara, M.O., Alçıçek, M.C., Németh, T., 2011. Stable isotope
1202 geochemical study of Pamukkale travertines: New evidences of low-temperature non-equilibrium calcite-
1203 water fractionation. *Sedimentary Geology* **238**(1-2), 191-212.

- 1204 Khatib, S., Rochette, P., Alçiçek, M.C., Lebatard, A.-E., Demory, F., Saos, T., 2014. Études stratigraphique,
1205 sédimentologique et paléomagnétique des travertins de Kocabaş, Bassin de Denizli, Anatolie, Turquie,
1206 contenant des restes fossiles quaternaires. *L'Anthropologie* **118**(1), 16-33.
- 1207 Kipata, M.L., Delvaux, D., Sebagenzi, M.N., Cailteux, J., Sintubin, M., 2013. Brittle tectonic and stress field
1208 evolution in the Pan-African Lufilian arc and its foreland (Katanga, DRC): from orogenic compression to
1209 extensional collapse, transpressional inversion and transition to rifting. *Geologica Belgica* **16**(1-2), 1-17.
- 1210 Koçyiğit, A., 2005. The Denizli graben-horst system and the eastern limit of western Anatolian continental
1211 extension: basin fill, structure, deformational mode, throw amount and episodic evolutionary history, SW
1212 Turkey. *Geodinamica Acta* **18**(3-4), 167-208.
- 1213 Laubach, S.E., Olson, J.E., Gale, J.F.W., 2004. Are open fractures necessarily aligned with maximum horizontal
1214 stresses? *Earth and Planetary Science Letters* **222**, 191-195.
- 1215 Lebatard, A.-E., Alçiçek, M.C., Rochette, P., Khatib, S., Vialet, A., Boulbes, N., Boulès, D.L., Demory, F.,
1216 Guipert, G., Mayda, S., Titov, V.V., Vidal, L., de Lumley, H., 2014. Dating the Homo erectus bearing
1217 travertine from Kocabaş (Denizli, Turkey) at least 1.1 Ma. *Earth and Planetary Science Letters* **390**, 8-18.
- 1218 Loveless, S., Bense, V., Turner, J., 2011. Fault architecture and deformation processes within poorly lithified rift
1219 sediments, Central Greece. *Journal of Structural Geology* **33**(11), 1554-1568.
- 1220 Maggi, M., Cianfarr, P., Salvini, F., Coelho de Lima, C., 2015. Staircase fractures in microbialites and the role
1221 of lamination-related mechanical anisotropy: The example of the Acquasanta Terme travertine deposits
1222 (central Italy). *GSA bulletin* **127**, 879-896.
- 1223 Martínez-Díaz, J.J., Hernández-Enrile, J.L., 2001. Using travertine deformations to characterize paleoseismic
1224 activity along an active oblique-slip fault: the Alhama de Murcia fault (Betic Cordillera, Spain). *Geologica*
1225 *Acta* **36**(3-4), 297-313.
- 1226 McKenzie, D., 1970. The plate tectonics of the Mediterranean region. *Nature* **226**, 239-243.
- 1227 Mesci, B.L., GURSOY, H., TATAR, O., 2008. The Evolution of Travertine Masses in the Sivas Area (Central
1228 Turkey) and Their Relationships to Active Tectonics. *Turkish Journal of Earth Sciences* **17**, 219-240.
- 1229 Nemeç, W., Steel, R.J., 1984. Alluvial and Coastal Conglomerates: Their Significant Features and Some
1230 Comments on Gravelly Mass-Flow Deposits. *Sedimentology of Gravels and Conglomerates* **10**, 1-31.
- 1231 Özkaymak, Ç., 2015. Tectonic analysis of the Honaz Fault (western Anatolia) using geomorphic indices and the
1232 regional implications. *Geodinamica Acta* **27**(2-3), 110-129.
- 1233 Özkul, M., Engin, B., Alçiçek, M.C., Koralay, T., Demirtaş, H., 2004. Thermoluminescence dating of
1234 Quaternary hot spring travertines and some implications on graben evolution, Denizli, Western Turkey. In:
1235 *32nd International Geological Congress, August 20–28, 2004, Florence, Italy*.
- 1236 Özkul, M., Gökgöz, A., Horvatinčić, N., 2010. Depositional properties and geochemistry of Holocene perched
1237 springline tufa deposits and associated spring waters: a case study from the Denizli Province, Western
1238 Turkey. *Geological Society, London, Special Publications* **336**(1), 245-262.
- 1239 Özkul, M., Gökgöz, A., Kele, S., Baykara, M.O., Shen, C.-C., Chang, Y.-W., Kaya, A., Hançer, M., Aratman,
1240 C., Akin, T., Örü, Z., 2014. Sedimentological and geochemical characteristics of a fluvial travertine: A case
1241 from the eastern Mediterranean region. *Sedimentology* **61**(1), 291-318.
- 1242 Özkul, M., Kele, S., Gökgöz, A., Shen, C.-C., Jones, B., Baykara, M.O., Föziz, I., Németh, T., Chang, Y.-W.,
1243 Alçiçek, M.C., 2013. Comparison of the quaternary travertine sites in the Denizli extensional basin based on
1244 their depositional and geochemical data. *Sedimentary Geology*.
- 1245 Özkul, M., Varol, B., Alçiçek, M.C., 2002. Depositional environments and petrography of the Denizli
1246 travertines. *Miner. Res. Expl. Bull.* **125**, 13-29.
- 1247 Piccardi, L., 2007. The ad 60 Denizli Basin earthquake and the apparition of Archangel Michael at Colossae
1248 (Aegean Turkey). *Geological Society, London, Special Publications* **273**(1), 95.
- 1249 Price, S.P., Scott, B., 1994. Fault-block rotations at the edge of a zone of continental extension; southwest
1250 Turkey. *Journal of Structural Geology* **16**(3), 381-392.
- 1251 Reading, H.G., 1996. *Sedimentary Environments; Processes, Facies and Stratigraphy*. London, Blackwell
1252 Science, 688 p.
- 1253 Röller, K., Trepmann, C.A., 2003. Stereo32 version 1.0.2. Ruhr Universität Bochum.
- 1254 Saller, A., Rushton, S., Buambua, L., Inman, K., McNeil, R., Dickson, J.A.D. 2016. Presalt stratigraphy and
1255 depositional systems in the Kwanza Basin, offshore Angola. *AAPG Bulletin*, 100, 1135–1164.
- 1256 Scholz, C.H., 1998. Earthquakes and friction laws. *Nature* **391**(37-42).
- 1257 Seyitoğlu, G., Scott, B.C., 1996. The cause of N-S extensional tectonics in western Turkey: Tectonic escape vs
1258 back-arc spreading vs orogenic collapse. *Journal of Geodynamics* **22**(1), 145-153.
- 1259 Sharp, I., Verwer, K., Ferreira, H., Lapponi, F., Snidero, M., Machado, V., Holtar, E., Swart, R., Marsh, J.,
1260 Gindre, L., Puigdefabregas, C., Fejerskov, M., 2013. Pre- and Post-Salt Non-Marine Carbonates of the
1261 Namibe Basin, Angola. *Programme and Abstract Volume: Microbial Carbonates in Space and Time:*
1262 *Implications for Global Exploration and Production. The Geological Society. 19-20 June, 2013.*
- 1263 Sibson, R., 1985. A note on fault reactivation. *Journal of Structural Geology* **7**(6), 751-754.

- 1264 Sintubin, M., Muchez, P., Similox-Tohon, D., Verhaert, G., Paulissen, E., Waelkens, M., 2003. Seismic
 1265 catastrophes at the ancient city of Sagalassos (SW Turkey) and their implications for seismotectonics in the
 1266 Burdur–Isparta area. *Geological Journal* **38**(3-4), 359-374.
- 1267 Soete, J., Kleipool, L.M., Claes, H., Claes, S., Hamaekers, H., Kele, S., Özkul, M., Foubert, A., Reijmer, J.J.G.,
 1268 Swennen, R., 2015. Acoustic properties in travertines and their relation to porosity and pore types. *Marine
 1269 and Petroleum Geology* **59**, 320-335.
- 1270 Taymaz, T., Price, S., 1992. The 1971 May 12 Burdur Earthquake sequence, SW Turkey - a synthesis of
 1271 seismological and geological observations. *Geophysical Journal International* **108**, 589–603.
- 1272 Temiz, U., Gökten, Y.E., Eikenberg, J., 2013. Strike-slip deformation and U/Th dating of travertine deposition:
 1273 Examples from North Anatolian Fault Zone, Bolu and Yeniçağ Basins, Turkey. *Quaternary International*
 1274 **312**(0), 132-140.
- 1275 ten Veen, J.H., Boulton, S.J., Alçiçek, M.C., 2009. From palaeotectonics to neotectonics in the Neotethys realm:
 1276 The importance of kinematic decoupling and inherited structural grain in SW Anatolia (Turkey).
 1277 *Tectonophysics* **473**(1–2), 261-281.
- 1278 Toker, E., Kayseri-Özer, M.S., Özkul, M., Kele, S., 2014. Depositional system and palaeoclimatic
 1279 interpretations of Middle to Late Pleistocene travertines: Kocabaş, Denizli, south-west Turkey.
 1280 *Sedimentology* **62**, 1360-1383.
- 1281 Topal, S., 2012. Denizli havzasındaki fayların tektonik jeomorfolojisi. Unpublished PhD thesis Pamukkale
 1282 University, 145 p. (in Turkish with English abstract). Unpublished PhD thesis.
- 1283 Topal, S., Özkul, M., 2014. Soft-Sediment Deformation Structures Interpreted as Seismites in the Kolankaya
 1284 Formation, Denizli Basin (SW Turkey). *The Scientific World Journal. Article ID 352654*, 13 p.
- 1285 van Ghendt, H.W., Holland, M., Urai, J.L., Loosveld, R., 2010. Evolution of fault zones in carbonates with
 1286 mechanical stratigraphy - Insights from scale models using layered cohesive powder. *Journal of Structural
 1287 Geology* **32**, 1375-1391.
- 1288 van Hinsbergen, D.J.J., Kaymakci, N., Spakman, W., Torsvik, T.H., 2010. Reconciling the geological history of
 1289 western Turkey with plate circuits and mantle tomography. *Earth and Planetary Science Letters* **297**(3-4),
 1290 674-686.
- 1291 Van Noten, K., Soete, J., Claes, H., Foubert, A., Özkul, M., Swennen, R., 2013. Fracture networks and strike-
 1292 slip deformation along reactivated normal faults in Quaternary travertine deposits, Denizli Basin, Western
 1293 Turkey. *Tectonophysics* **588**, 154-170.
- 1294 Van Noten, K., Van Baelen, H., Sintubin, M., 2012. The complexity of 3D stress-state changes during
 1295 compressional tectonic inversion at the onset of orogeny. In: Healy, D., Butler, R.W.H., Shipton, Z.K.,
 1296 Sibson, R.H. (Eds.), *Faulting, Fracturing, and Igneous Intrusion in the Earth's crust*. Geological Society,
 1297 London, Special Publications 367, 51-69.
- 1298 Verhaert, G., Similox-Tohon, D., Vanduycke, S., Sintubin, M., Muchez, P., 2006. Different stress states in the
 1299 Burdur-Isparta region (SW Turkey) since Late Miocene times: a reflection of a transient stress regime.
 1300 *Journal of Structural Geology* **28**, 1067–1083.
- 1301 Wallace, R.E., 1951. Geometry of shearing stress and relation to faulting. *Journal of Geology* **69**, 118–130.
- 1302 Wang, Z., Meyer, M.C., Gliganic, L.A., Hoffmann, D.L., May, J.-H., 2017. Timing of fluvial terrace formation
 1303 and concomitant travertine deposition in the upper Sutlej River (Tirthapuri, southwestern Tibet) and
 1304 paleoclimatic implications. *Quaternary Science Reviews* **169**, 357-377.
- 1305 Westaway, R., 1990. Block rotation in western Turkey, 1. Observational evidence. *J. of Geo. Res.* **95**, 19857-
 1306 19884.
- 1307 Westaway, R., 1993. Neogene evolution of the Denizli region of western Turkey. *Journal of Structural Geology*
 1308 **15**, 37-53.
- 1309 Westaway, R., Guillou, H., Yurtmen, S., Demir, T., Scaillet, S., Rowbotham, G., 2005. Constraints on the
 1310 timing and regional conditions at the start of the present phase of crustal extension in western Turkey, from
 1311 observations in and around the Denizli region. *Geodinamica Acta* **18**(3-4), 209-238.
- 1312 Westaway, R., Pringle, M., Yurtmen, S., Demir, T., Bridgland, D., Rowbotham, G., Maddy, D., 2003. Pliocene
 1313 and Quaternary surface uplift of western Turkey revealed by long-term river terrace sequences. *Current
 1314 Science* **84**(8), 1090-1101.
- 1315 Yalçiner, C.C., 2013. Investigation of the subsurface geometry of fissure-ridge travertine with GPR, Pamukkale,
 1316 western Turkey. *J. Geophys. Eng.* **10**. 035001, 10pp.